



The effect of greenhouse gases concentration and urbanization on future temperature over Guangdong-Hong Kong-Macao Greater Bay Area in China

Zhiyuan Zheng^{1,2,3,4} · Dongdong Yan^{5,7} · Xiaohang Wen⁶ · Zhigang Wei⁵ · Jieming Chou⁵ · Yan Guo⁵ · Xian Zhu^{1,2,3} · Wenjie Dong^{1,2,3,4}

Received: 7 September 2021 / Accepted: 7 December 2021 / Published online: 13 February 2022
© The Author(s), under exclusive licence to Springer-Verlag GmbH Germany, part of Springer Nature 2022

Abstract

Relative contributions of greenhouse gases (GHGs) concentration and land use/cover (LULC) change induced by urbanization on future temperature over the Guangdong-Hong Kong-Macao Greater Bay Area in China under different climate scenarios are investigated in this study. The Weather Research and Forecasting model is used to downscale the future mean and extreme temperature using the Representative Concentration Pathways (RCP) 4.5&8.5 simulations from the Community Earth System Model. Results show that GHGs concentration is the key dominate factor for future mean and extreme temperature over the Greater Bay Area in the next 10–30 years, LULC change (urbanization) has relative slight effect on the future regional temperature. On the urban local scale, the LULC change in urban area has an obvious warming effect on urban local temperature under future different GHGs concentration scenarios. The regional-averaged annual mean surface air temperature (SAT) of urban area will increase 0.51 °C (0.73 °C), 0.83 °C (1.17 °C) and 1.26 °C (1.74 °C) resulting from the combined contributions of urbanization and GHGs forcing for the year of 2030, 2040, and 2050 under RCP4.5(RCP8.5) scenario, respectively. The contributions of the GHGs forcing are 0.33 °C (0.53 °C), 0.66 °C (1.00 °C) and 1.12 °C (1.58 °C), the urbanization forcing are 0.18 °C (0.20 °C), 0.17 °C (0.17 °C) and 0.14 °C (0.16 °C). Same as regional-averaged annual mean SAT, for the extreme high- and low-temperature, the contribution of GHGs forcing is more important than that of the urbanization forcing. The extreme temperatures are more sensitively to GHGs concentration under RCP8.5 scenario than that under RCP4.5, especially for the extreme low-temperature. GHGs are the most important factor for dominating the future mean and extreme temperature of the Greater Bay Area.

Keywords Guangdong-Hong Kong-Macao Greater Bay Area · Future temperature · Greenhouse gases concentration · Urbanization · Land use/cover change

✉ Dongdong Yan
yan_dongdong@mail.bnu.edu.cn

✉ Wenjie Dong
dongwj3@mail.sysu.edu.cn

¹ School of Atmospheric Sciences, Sun Yat-Sen University, Zhuhai 519082, China

² Key Laboratory of Tropical Atmosphere-Ocean System (Sun Yat-Sen University), Ministry of Education, Zhuhai 519082, China

³ Southern Marine Science and Engineering Guangdong Laboratory (Zhuhai), Zhuhai 519082, China

⁴ Guangdong Provincial Field Observation and Research Station for Climate Environment and Air Quality Change in the Pearl River Estuary, Guangzhou 510275, China

⁵ State Key Laboratory of Earth Surface Processes and Resource Ecology, Faculty of Geographical Science, Beijing Normal University, Beijing 100875, China

⁶ Plateau Atmosphere and Environment Key Laboratory of Sichuan Province, School of Atmospheric Sciences, Chengdu University of Information Technology, Chengdu 610225, China

⁷ Shenzhen Urban Public Safety and Technology Institute, Shenzhen 518046, China

1 Introduction

According to the Intergovernmental Panel on Climate Change (IPCC) assessment reports (IPCC AR4, 2007; IPCC AR5, 2013; IPCC AR6, 2021), human activities significantly affect global and regional weather and climate. Greenhouse gases (GHGs) emission and Land use/cover (LULC) change are two important forcing factors that have great impact on weather and climate (Lejeune et al. 2017; Huang et al. 2020; IPCC AR6, 2021; Sun et al. 2021; Wang et al. 2021). Focus on the urban area, global warming and urbanization are the two major drivers of the warming environment in the city (Yang et al. 2011; Sun et al. 2014, 2021; Bassett et al. 2020; Kong et al. 2020; Wang et al. 2020, 2021). Urbanization, one form of human-induced LULC change, plays an important role in human-induced weather and climate change (temperature and precipitation) on the regional/local and global scales through altering land-atmosphere interactions because of its impacts on atmospheric dynamics, thermodynamics, energy exchanges, cloud microphysics, and atmospheric composition (Oke 1982; Shepherd 2005; Miao et al. 2009; Zhang et al. 2010; Chen et al. 2011; Gao et al. 2011, 2012, 2021; Feng et al. 2012, 2013, 2014; Wang et al. 2012, 2013, 2015; Yang et al. 2012, 2021; Mahmood et al. 2014; Shimadera et al. 2015; Chen and Frauenfeld 2016; Perugini et al. 2017; Kong et al. 2020; Han et al. 2020; Liu et al. 2021; Sun et al. 2021). Climate change and LULC change also could alter the groundwater recharge areas and the surface and subsurface flows in the river basin (Lamichhane and Shakya 2019a, 2019b). Therefore, Mahmood et al. (2014) suggested that dynamic urbanization process and its influence should be considered in future Earth modeling systems.

Nowadays, China is in the stage of rapid urbanization accompanied with more and more people moving from rural to urban (Gong et al. 2012). Therefore, urbanization is not only an issue of Socio-Economic development, but also an issue of Human-Earth system interaction. Urbanization could alter the original underlying surface biophysical properties, such as surface albedo and emissivity, surface roughness, drag coefficient, friction, thermal conductivity and diffusivity, and in turn it could affect urban local and regional environment and climate by altering ground surface substance and energy exchange and balance (Shepherd 2005; Kaufmann et al. 2007; Yang et al. 2012; Mahmood et al. 2014; Perugini et al. 2017; Sun et al. 2021; Wang et al. 2021). As China's reform and opening up are deepened over the past 40 years, urbanization has already received plenty of attention for its impact on weather and climate, such as in the Beijing-Tianjin-Hebei region, the Yangtze River Delta region, the Pearl River Delta region (Miao et al. 2009; Wang et al. 2012, 2013, 2015, 2019, 2020, 2021; Feng et al. 2014; Zhang et al. 2010; Gao et al. 2021; Sun et al. 2021;

Yang et al. 2021). The Weather Research and Forecasting (WRF) model is the main tool and has been widely used to investigate the effect and physical mechanism of the LULC change, Anthropogenic Heat Release (AHR)/Urban Heat Island (UHI) and urban aerosol on weather and climate in China (Miao et al. 2009; Zhang et al. 2010; Gao et al. 2011, 2012, 2021; Feng et al. 2012, 2013, 2014; Wang et al. 2012, 2013, 2015; Yang et al. 2012; Chen and Frauenfeld 2016; Kong et al. 2020; Han et al. 2020; Liu et al. 2021).

The Guangdong-Hong Kong-Macao Greater Bay Area (Greater Bay Area) comprises the two Special Administrative Regions of Hong Kong and Macao, and the nine municipalities of Guangzhou, Shenzhen, Zhuhai, Foshan, Huizhou, Dongguan, Zhongshan, Jiangmen and Zhaoqing in Guangdong Province. The total area is around 56,000 km². At end 2019, the total population is over 72 million. The development of the Greater Bay Area is accorded the status of key strategic planning in the country's development blueprint, having great significance in the country's implementation of innovation-driven development and commitment to reform and opening-up. The objectives are to further deepen cooperation amongst Guangdong, Hong Kong and Macao, fully leverage the composite advantages of the three places, facilitate in-depth integration within the region, and promote coordinated regional economic development, with a view to developing an international first-class bay area ideal for living, working and travelling. That integration would further prop China's infrastructure and connectivity programs like the Belt and Road Initiative as well as strengthen the supply chain industry in higher-tech manufacturing and services. On 1 July 2017, witnessed by President Xi Jinping, the National Development and Reform Commission and the governments of Guangdong, Hong Kong and Macao signed the Framework Agreement on Deepening Guangdong-Hong Kong-Macao Cooperation in the Development of the Greater Bay Area in Hong Kong (Framework Agreement on Deepening Guangdong-Hong Kong-Macao Cooperation in the Development of the Greater Bay Area). The Framework Agreement sets out the goals and principles of cooperation and establishes the key cooperation areas in the development of the Greater Bay Area (Guangdong-Hong Kong-Macao Greater Bay Area—Overview).

The Greater Bay Area, one of the most important and developed areas in China, is located in southern China with a typical East Asian tropical monsoon climate regime. As a result of national development strategy, the Greater Bay Area is undergoing a rapid process of urbanization, industrialization and economic growth, which causes an obvious expansion of urban areas and in turn changes the regional and local climate and environment. Since the Greater Bay Area is or will be an important economy center, future climate projection within this region is very important for the safety of people's lives and property as well as the social

development. However, it is also extremely unbalanced in terms of urban areas. Although many previous studies have indicated that urbanization has significant impacts on weather, climate and environment in the different spatial-temporal scales (Shepherd 2005; Zhang et al. 2010; Chen et al. 2011; Gao et al. 2011, 2012, 2021; Yang et al. 2011, 2012; Feng et al. 2012, 2013, 2014; Wang et al. 2012, 2016, 2021; Argüeso et al. 2014; Sun et al. 2014; Shimadera et al. 2015; Liao et al. 2018; Ye et al. 2018; Lamichhane and Shakya 2019a, 2019b, 2020; Bassett et al. 2020; Shi et al. 2021; Yang et al. 2021), projections of future weather, climate and environment have rarely been investigated in the Greater Bay Area under the increasing urban land areas and different GHGs concentration scenarios, especially the extreme high and low temperature. Although the LULC change forcing has been included in many climate models, as shown in Coupled Model Intercomparison Project Phase 5 (CMIP5), the urban fraction usually still remains constant over time (Di Vittorio et al. 2014). The contribution of dynamic urban forcing on the future climate should be considered in the climate prediction (Mahmood et al. 2014; Wang et al. 2020; Sun et al. 2021).

In this study, the WRF version 3.9.1 (Skamarock et al. 2008) was used to investigate the effects of GHGs concentration and urbanization on future temperature in the Greater Bay Area under the RCP4.5&8.5 scenarios. We use the WRF model to dynamically downscale the Greater Bay Area future climate projections and aim to understand the following questions: (1) What are the relative contributions of the GHGs concentration and the LULC change induced by urbanization on the future temperature in the Greater Bay Area under different future climate scenarios? (2) What are the future temperature projections of the extreme hot and cold event in the Greater Bay Area? (3) What is/are the dominate factor(s) for the future temperature in the Greater Bay Area during the next 10–30 years?

The rest of the paper is organized as follows. In Sect. 2, model, data and numerical experimental design used in this study are introduced. In Sect. 3, we present the results of the WRF simulation and reveal the qualitative and quantitative contributions of GHGs concentration and urbanization to the future temperature in the Greater Bay Area under different future climate scenarios. Conclusion and discussions are provided in Sect. 4.

2 Model, data and experimental design

2.1 The WRF model

The WRF model version 3.9.1 (Skamarock et al. 2008) is used in this study. Detailed description of the employed spatial domain, physical parameterization schemes, initial

conditions, and lateral boundary conditions, is given as follow. Focusing on the Greater Bay Area, the numerical simulations are conducted over two-nesting domains. As shown in Fig. 1 and Table 1, The largest domain (d01) covers most of the southern China centered at 113.83°E and 21.92°N, and the innermost domain (d02) covers the Greater Bay Area with the center at 114.00°E and 21.76°N. The two domains have the dimensions of 68 × 65 (east-west, north-south) grid cell for the d01 and 70 × 64 (east-west, north-south) grid cell for the d02, respectively. The horizontal grid resolutions are 18 km for d01 and 6 km for d02. Land use resolution are both 0.25°. The vertical levels are set to 29 with the model top at 50 hPa in each domain.

The parameterization schemes of physical processes (Table 2) are chosen referring to some previous studies (Gao et al. 2011, 2012, 2021; Feng et al. 2012, 2013, 2014; Wang et al. 2012; Chen and Frauenfeld 2016). The shortwave radiation parameterization scheme is the RRTMG shortwave scheme (Iacono et al. 2008), and the RRTM scheme is used for the longwave radiation parameterization (Mlawer et al. 1997). The microphysics parameterization scheme used is the Purdue Lin Scheme (Chen and Sun 2002). The cumulus convective parameterization used is the Kain–Fritsch scheme (Kain 2004). The Yonsei University (YSU) scheme (Hong et al. 2006) is used for the Planetary boundary layer (PBL) parameterization. The Noah Land Surface model (Tewari et al. 2004) coupled with the single-layer UCM (Chen et al. 2011) is used for land surface processes parameterization

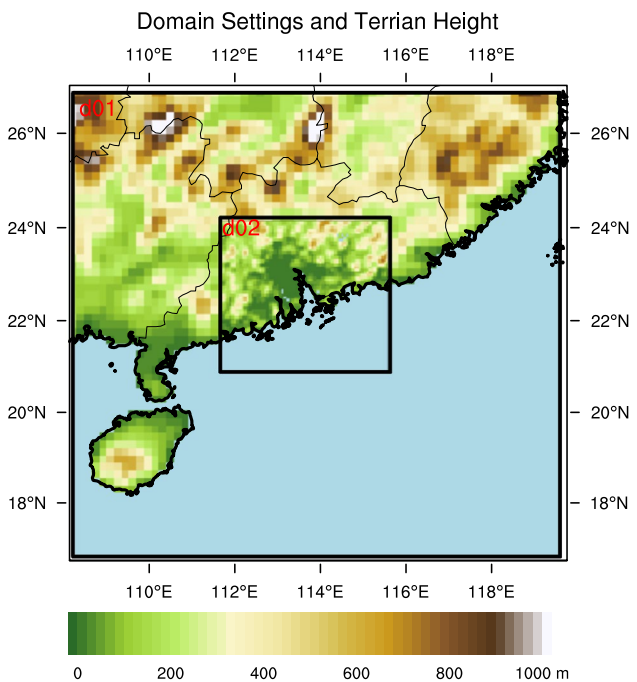


Fig. 1 The two nested domains with 18 km (d01) and 6 km (d02) grid used for the numerical simulations in the WRF model

Table 1 Model configuration information

| Grid ID | Domain center (Lon, Lat) | Number of points (Lon × Lat) | Horizontal grid resolution (km) | Integration time step (s) | Land use resolution (°) |
|---------|--------------------------|------------------------------|---------------------------------|---------------------------|-------------------------|
| 1 | 113.83°E, 21.92°N | 68 × 65 | 18 | 60 | 0.25 |
| 2 | 114.00°E, 21.76°N | 70 × 64 | 6 | 60 | 0.25 |

Table 2 Parameterization scheme of the physical processes in the WRF model configuration

| Physical processes | Parameterization scheme | References |
|--------------------------|----------------------------------|-----------------------|
| Microphysics | Purdue Lin Scheme | Chen and Sun (2002) |
| Longwave radiation | RRTM scheme | Mlawer et al. (1997) |
| Shortwave radiation | RRTMG shortwave | Iacono et al. (2008) |
| Cumulus parameterization | Kain–Fritsch scheme | Kain (2004) |
| Planetary boundary layer | Yonsei University scheme | Hong et al. (2006) |
| Land surface | Noah land surface model | Tewari et al. (2004) |
| Urban surface | Single-layer urban canopy model | Chen et al. (2011) |
| Surface layer | Revised MM5 Monin–Obukhov scheme | Jiménez et al. (2012) |

Table 3 Numerical experimental design

| Experiment | Urban canopy | Forcing data | Land use categories |
|------------|--------------|--------------------------|---------------------------------|
| HIST | Yes | NCAR-CESM2WRF Historical | 20 MODIS |
| S1 | Yes | NCAR-CESM2WRF RCP4.5 | 20 MODIS |
| S2 | Yes | NCAR-CESM2WRF RCP8.5 | 20 MODIS |
| S1_EXP | Yes | NCAR-CESM2WRF RCP4.5 | 20 MODIS + expanded Urban areas |
| S2_EXP | Yes | NCAR-CESM2WRF RCP8.5 | 20 MODIS + expanded urban areas |

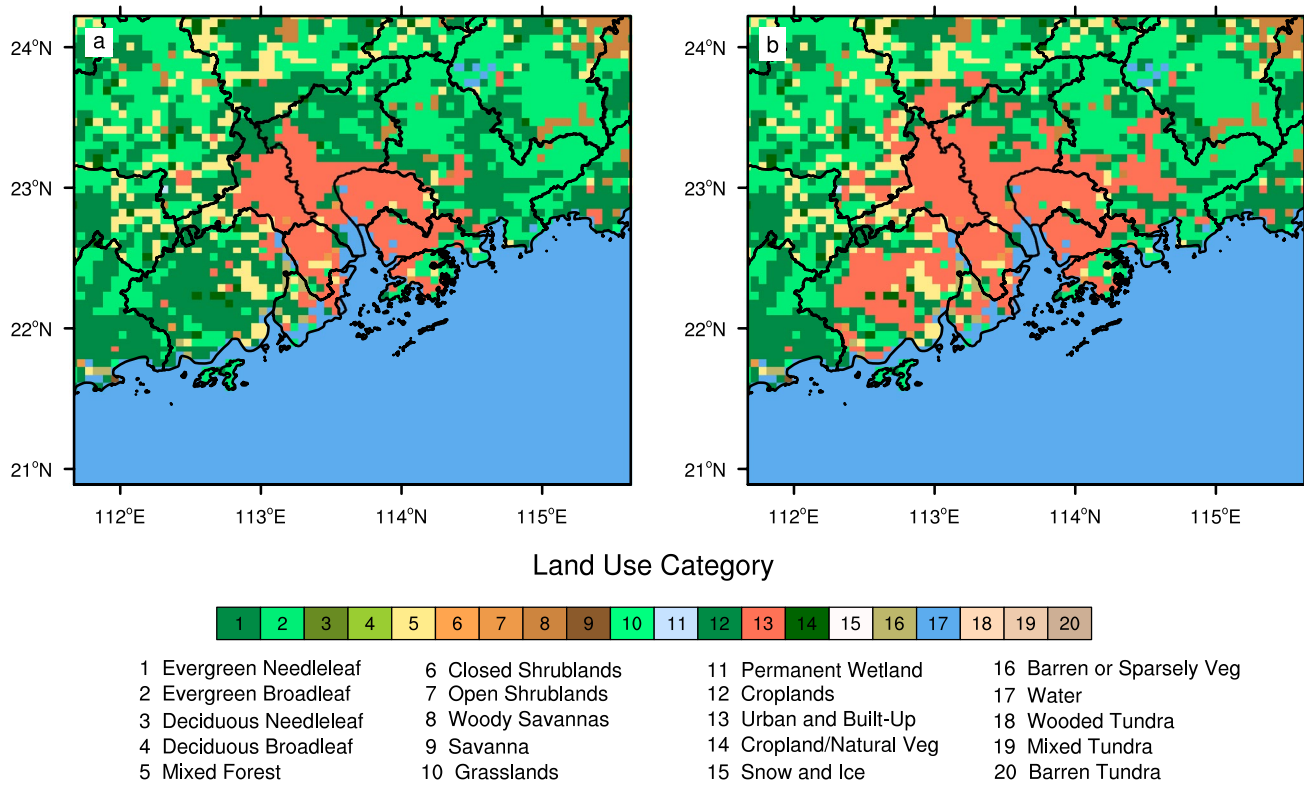
**Fig. 2** Land use and coverage for the present and future specified in the WRF model. The diagrams in **(a, b)** are for **a** the present and **b** the next 30 years in the future, respectively

Table 4 Land use categories and their parameters in MODIS20 used in this study

| Index | Land categories | ALBD | SLMO | SFEM | SFZ0 | THERIN | SFHC |
|-------|------------------------------|------|------|-------|------|--------|----------|
| 1 | Evergreen needleleaf forest | 12 | 0.3 | 0.95 | 50 | 4 | 2.92E+06 |
| 2 | Evergreen broadleaf forest | 12 | 0.5 | 0.95 | 50 | 5 | 2.92E+06 |
| 3 | Deciduous needleleaf forest | 14 | 0.3 | 0.94 | 50 | 4 | 2.50E+06 |
| 4 | Deciduous broadleaf forest | 16 | 0.3 | 0.93 | 50 | 4 | 2.50E+06 |
| 5 | Mixed Forest | 13 | 0.3 | 0.97 | 50 | 4 | 4.18E+06 |
| 6 | Closed shrubland | 22 | 0.1 | 0.93 | 5 | 3 | 2.08E+06 |
| 7 | Open Shrubland | 20 | 0.15 | 0.95 | 6 | 3 | 2.08E+06 |
| 8 | Woody Savanna | 22 | 0.1 | 0.93 | 5 | 3 | 2.08E+06 |
| 9 | Savanna | 20 | 0.15 | 0.92 | 15 | 3 | 2.50E+06 |
| 10 | Grassland | 19 | 0.15 | 0.96 | 12 | 3 | 2.08E+06 |
| 11 | Permanents Wetland | 14 | 0.42 | 0.95 | 30 | 5.5 | 3.55E+06 |
| 12 | Cropland | 17 | 0.3 | 0.985 | 15 | 4 | 2.50E+06 |
| 13 | Urban and Built-up | 15 | 0.1 | 0.88 | 80 | 3 | 1.89E+06 |
| 14 | Cropland/Natural Mosaic | 18 | 0.25 | 0.98 | 14 | 4 | 2.50E+06 |
| 15 | Snow and Ice | 55 | 0.95 | 0.95 | 0.1 | 5 | 9.00E+25 |
| 16 | Barren or Sparsely Vegetated | 25 | 0.02 | 0.9 | 1 | 2 | 1.20E+06 |
| 17 | Water | 8 | 1 | 0.98 | 0.01 | 6 | 9.00E+25 |
| 18 | Wooded Tundra | 15 | 0.5 | 0.93 | 30 | 5 | 9.00E+25 |
| 19 | Mix Tundra | 15 | 0.5 | 0.92 | 15 | 5 | 9.00E+25 |
| 20 | Barren Tundra | 25 | 0.02 | 0.9 | 10 | 2 | 1.20E+06 |

USGS LU categories and their physical parameters are taken from LANDUSE.TBL in the WRF model. Parameters from left to right are: albedo (ALBD %), soil moisture availability (SLMO $\times 100\%$), surface emissivity (SFEM %), surface roughness length ($SFZ0 \times 10^{-2}$ m), thermal inertia ($THERIN \times 4.184 \times 10^2$ J/m 2 K $^{1/2}$), and surface heat capacity ($SFHC \times 10^6$ J/m 3 K), respectively

and land–atmosphere interactions. The surface layer scheme is the revised MM5 Monin–Obukhov scheme (Jiménez et al. 2012).

2.2 Data

The Climatic Research Unit gridded Time Series (CRU TS) dataset version 4 is employed as the observational data to evaluate the performance of the WRF model. The CRU TS is one of the most widely used observed climate datasets and is produced by UK’s National Centre for Atmospheric Science (NCAS) at the University of East Anglia’s Climatic Research Unit (CRU). The CRU TS Version 4 features an improved interpolation process, which delivers full traceability back to station measurements (Harris et al. 2020). We chose the temperature datasets on $0.5^\circ \times 0.5^\circ$ grid of the CRU TSv4 to evaluate the performance of WRF in the historical period.

Previous study has indicated that the Community Earth System Model (CESM) is the best Global Climate Model (GCM) in terms of simulating the observed temperature and precipitation at the global scale in phase 5 of the Coupled Model Intercomparison Experiment (CMIP5) compared

with other GCMs (Knutti and Sedlacek 2013). Moreover, the CESM can well reproduce the climate variability in China (Chen and Frauenfeld 2014a, b). Therefore, the “NCAR CESM Global Bias-Corrected CMIP5 Output to Support WRF/MPAS Research” dataset (CESM2WRF) is used as lateral boundary and initial conditions for WRF downscaling of the past and future climate projections in this study (Monaghan et al. 2014). As indicated in Monaghan et al. (2014), the CESM2WRF dataset includes global bias-corrected climate model output data from the CESM version 1 of the National Center for Atmospheric Research (NCAR) that participated in CMIP5. This dataset contains all the variables needed for initial and boundary conditions for regional simulations. All the variables are provided in the Intermediate File Format to WRF, which have been interpolated to 26 pressure levels and provided in files at six hourly intervals. All of the variables also have been bias-corrected using the European Centre for Medium-Range Weather Forecasts (ECMWF) Interim Reanalysis (ERA-Interim, Dee et al. 2011) fields for 1981–2005 according to the method given in Bruyère et al. (2014). We choose the RCP4.5&8.5 scenarios for future climate projection. According to the

work of Stocker et al. (2014), by 2050, carbon dioxide (CO_2) concentration will reach 500 ppm under RCP4.5 scenario, but more than 600 ppm under RCP8.5 scenario. Moderate emission (RCP4.5) and high emission (RCP8.5) are analyzed in this study.

2.3 Numerical experimental design

In this study, besides the influence of GHGs concentration, we only consider the effect of LULC change during the urbanization processes on the future temperature, except for the effects of anthropogenic aerosol and anthropogenic heat produced by expanded human activities. Five numerical experiments were conducted to investigate the effect of LULC change produced by urbanization and GHGs

concentration on future temperature in the Greater Bay Area (Table 3). The five numerical experiments include:

- (1) historical experiment (HIST): A historical run (1980–2005) forced with the land cover condition in 2002 (Fig. 2a), which is prescribed using the Moderate-resolution Imaging Spectroradiometer (MODIS) 20-category land use data. There are 325 urban grid points within this region in this scenario, approximately 117,000 km²;
- (2) future RCP-4.5 experiment (S1): A RCP4.5 scenario run (2020–2050) forced with 2002 land cover condition (Fig. 2a);

Table 5 Definitions of temperature indices used in this study

| Index | Index name | Definition | Unit |
|-------|--------------------------|---|------|
| 1 | Mean temperature | Mean 2-m surface air temperature in a year | °C |
| 2 | Extreme high-temperature | 90th percentile 2-m surface air temperature in a year | °C |
| 3 | Extreme low-temperature | 10th percentile 2-m surface air temperature in a year | °C |

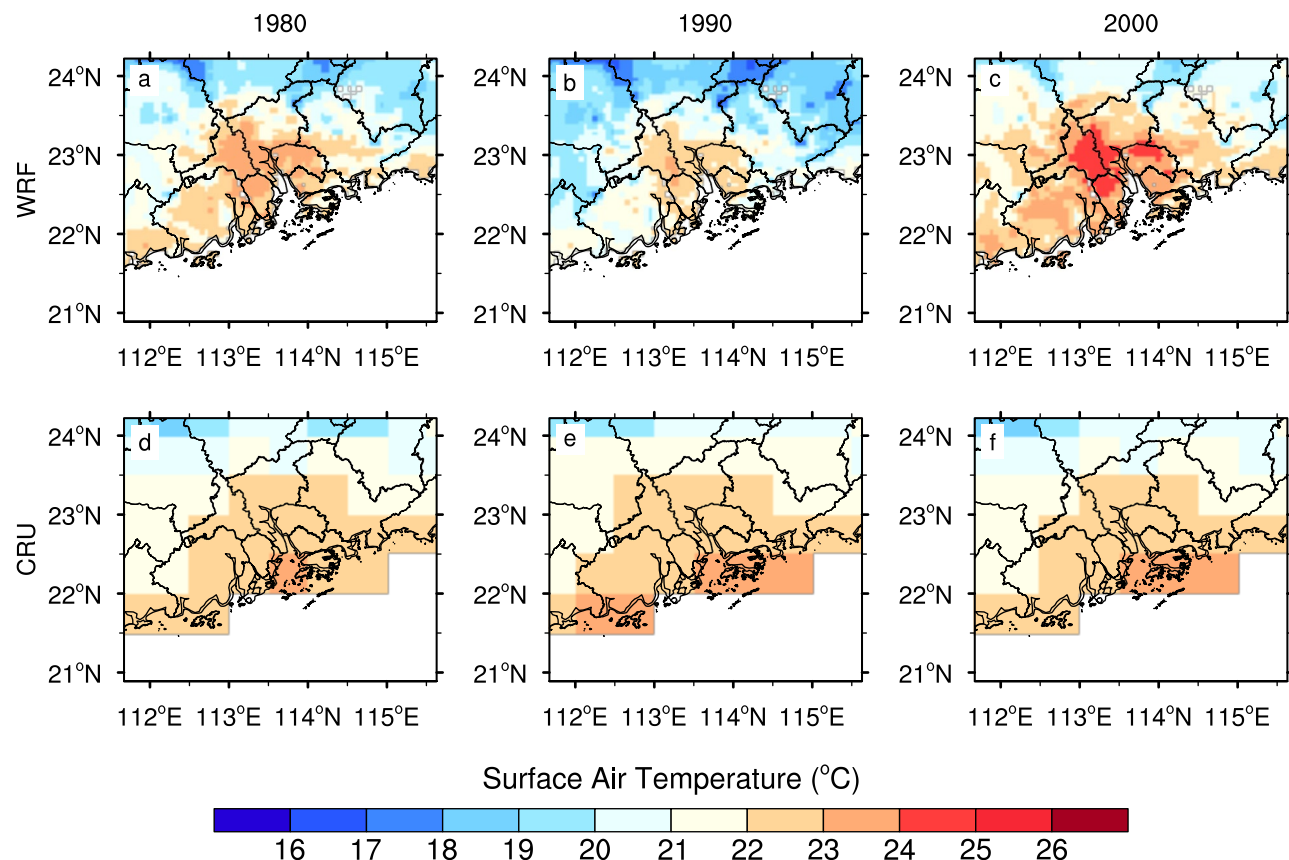


Fig. 3 Comparisons of annual mean surface air temperature between the observation and simulation. The top row is the simulation from WRF, and the bottom row is the observation of the CRU TSv4. The

diagrams in (a–f) are for **a**, **d** the year of 1980, **b**, **e** the year of 1990, and **c**, **f** the year of 2000, respectively

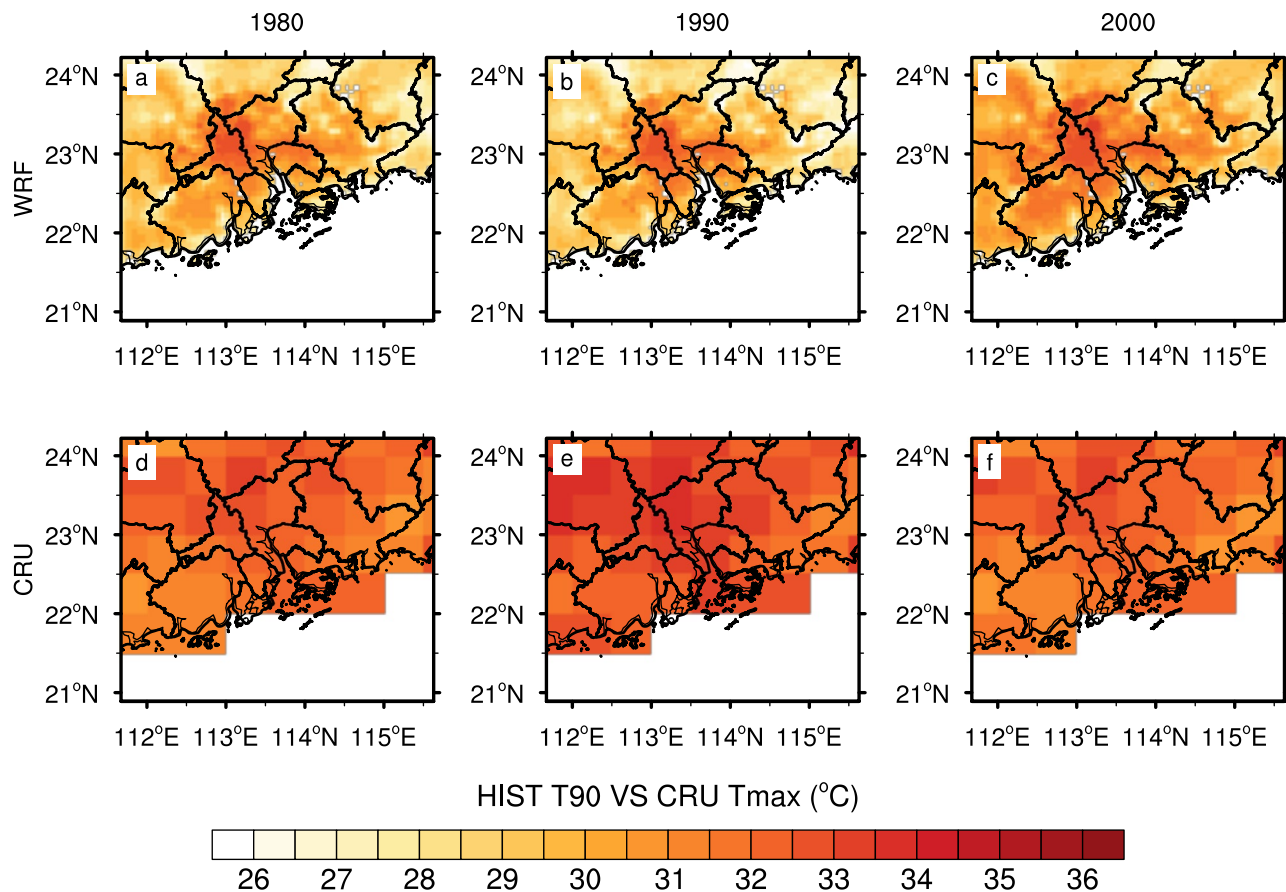


Fig. 4 Same as Fig. 3, but for the T90

- (3) future RCP-8.5 experiment (S2): A RCP8.5 scenario run (2020–2050) forced with 2002 land cover condition (Fig. 2a);
- (4) future URB-4.5 experiment (S1_EXP): A RCP4.5 scenario run (2020–2050) forced with future urbanized expanded land cover condition (Fig. 2b). There are 575 urban grid points within this region in this scenario, approximately 20,700 km²;
- (5) future URB-8.5 experiment (S2_EXP): A RCP8.5 scenario run (2020–2050) forced with future urbanized expanded land cover condition (Fig. 2b), same as in the S1_EXP experiment.

The above five experimental settings are basically the same, except for the underlying surface properties and their corresponding leaf area index and vegetation coverage. Land use categories and their parameters in MODIS20 used in this study are shown in Table 4. The Greater Bay Area, including the two Special Administrative Regions of Hong Kong and

Macao, and the nine municipalities of Guangzhou, Shenzhen, Zhuhai, Foshan, Huizhou, Dongguan, Zhongshan, Jiangmen and Zhaoqing in Guangdong province, are all developed rapidly referring to Framework Agreement on Deepening Guangdong-Hong Kong-Macao Cooperation in the Development of the Greater Bay Area. Guided by the Framework Agreement on Deepening Guangdong-Hong Kong-Macao Cooperation in the Development of the Greater Bay Area (Framework Agreement on Deepening Guangdong-Hong Kong-Macao Cooperation in the Development of the Greater Bay Area), considered the effect of the topographic and geomorphic features of the Greater Bay Area, the original farmland and the areas with a terrain height of less than 50 m in the flat areas are all modified to urban underlying surface around the major nine cities within this region. Compared with Fig. 2a, the expanded urban area is 9000 km² in total, the coral areas shown in Fig. 2b. Figure 2b shows the fastest development scenario of urbanization in the Greater Bay Area for the next 30–50 years. According

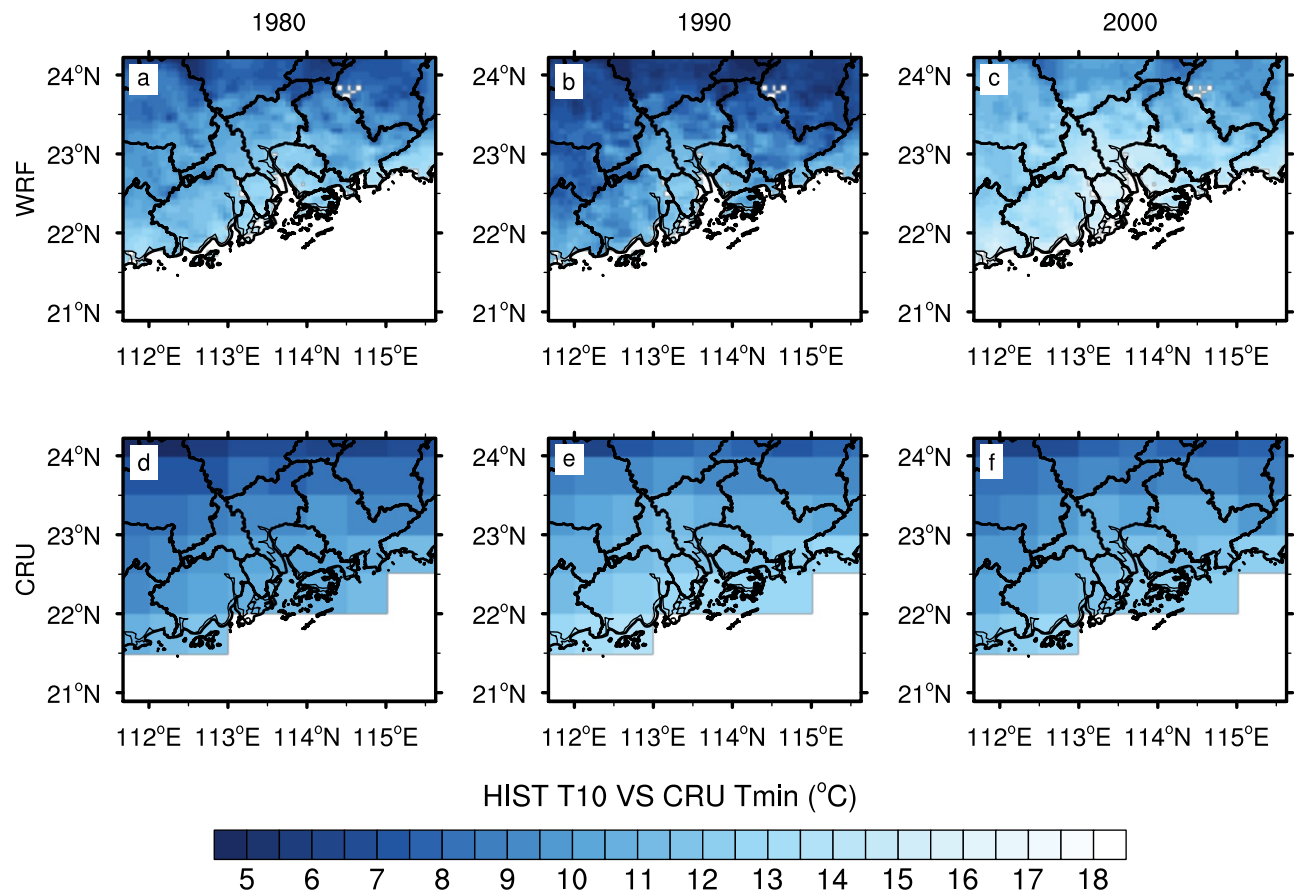


Fig. 5 Same as Fig. 3, but for the T10

to Communiqué of the Seventh National Population Census from National Bureau of Statistics of China (Communiqué of the Seventh National Population Census (No. 3) (stats.gov.cn)), there are about 80 million people living in the Greater Bay Area in 2020. Based on this population density, the maximum population supporting capacity of the Greater Bay Area will be approximately 100 million in the future.

The climatology is the averaged value during the period of 1980–2005 from the historical simulations. The difference between S1 (S2) and HIST represents the future temperature change due to the GHGs forcing under the RCP4.5 (RCP8.5) scenario, while the difference between S1_EXP (S2_EXP) and HIST represents the future climate change due to the combined influences of GHGs forcing and LULC change induced by urbanization under the RCP4.5 (RCP8.5) scenario. The difference between S1_EXP (S2_EXP) and S1 (S2) shows the impact of LULC change induced by urbanization on the future temperature. We chose three special years as historical periods (1980, 1990 and 2000) and three special years as future scenarios (2030, 2040 and 2050),

respectively. The RCP4.5 scenario represents the future climate scenario for moderate emissions, and the RCP8.5 represents the future climate for high emissions. The different special years of 2030, 2040 and 2050 represent different climate scenarios under the RCP4.5&8.5 forcing run in the future. It is worth noting that the years of 2030, 2040 and 2050 are not the ones in the factual world, but the states of climate scenarios hypothesized in the future under RCP4.5&8.5 scenarios. The first 2 months of each experiment (November and December) are considered as the spin-up period and only the next year's results are used for analysis.

3 Results

3.1 Evaluation of WRF downscaling

In this study, three indices, including annual mean 2-m surface air temperature (SAT), annual extreme high-temperature

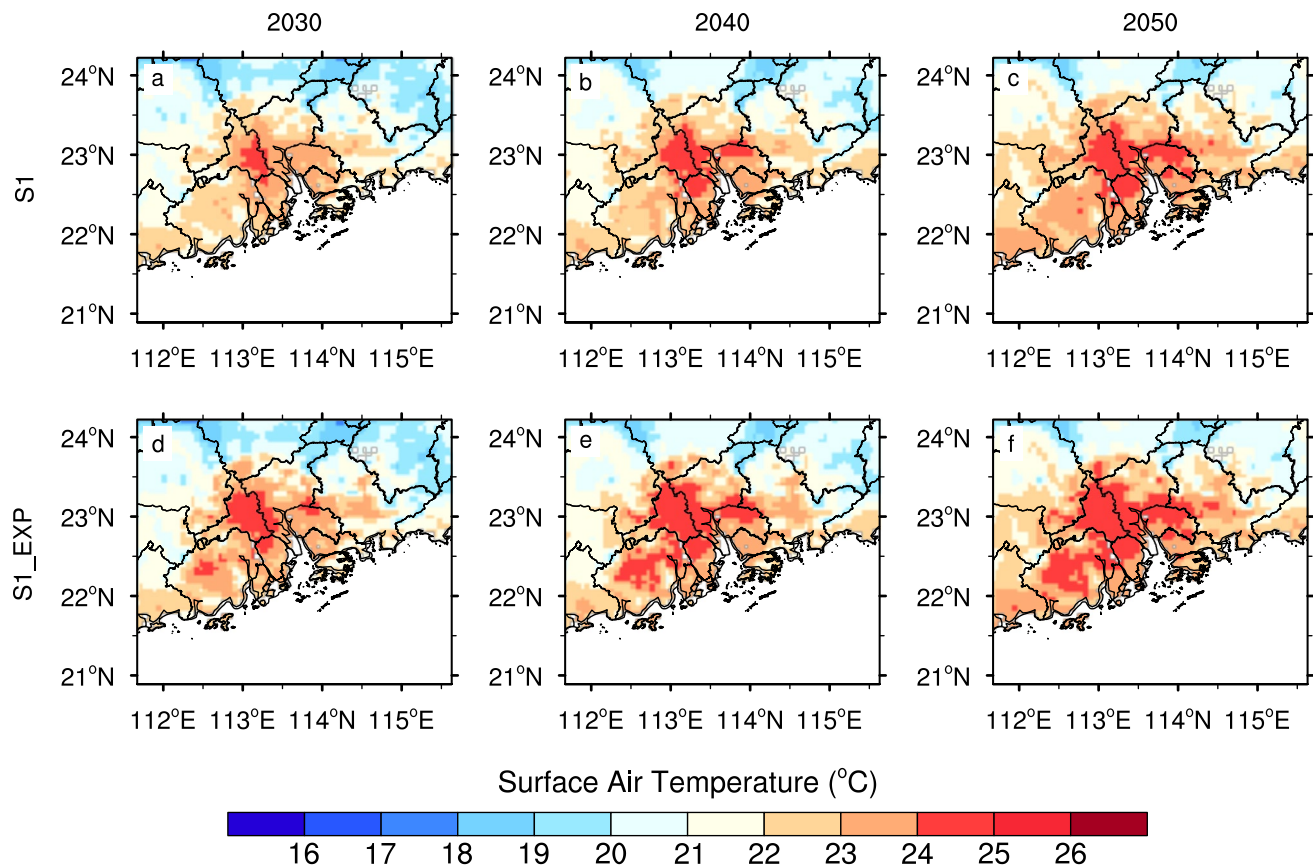


Fig. 6 Comparisons of annual mean surface air temperature between the S1 and S1_EXP experiment for different future climate scenarios under the RCP4.5 scenario. The top row is the result of S1, and the

bottom row is the result of S1_EXP. The diagrams in (a–f) are for **a**, **d** the year of 2030, **e** the year of 2040, and **c**, **f** the year of 2050, respectively

(T90) and annual extreme low-temperature (T10), are chosen to evaluate the performance of the developed WRF downscaling modeling system. Definitions of these three temperature indices are shown in Table 5. As shown in Fig. 3, the WRF model exhibits a great simulated ability for the annual mean SAT. The simulated spatial patterns of annual mean SAT are essentially consistent with the observations in the years of 1980, 1990 and 2000 accompanied with gradually decrease from south to north. The model successfully reproduces the influence of complex topography (hills and mountainous landforms) on annual mean SAT. The low temperature zone is located in the north of the Guangdong Province, and the high temperature zone is located in the Pearl River Delta Region. The extremum center locations of maximum and minimum SAT can also be well depicted.

Same as the annual mean SAT, the annual T90 (Fig. 4) and T10 (Fig. 5) in a year can also be well reproduced by WRF model. Spatial patterns and extremum centers of T90 and T10 are essentially consistent with the observations. In

the past few decades, with the increase of CO₂ concentration, the thresholds for T90 and T10 have increased in the Greater Bay Area (Figs. 4d–f and 5d–f). The area of higher temperature has also increased within this region. These evolution features are also well reproduced by the model, as shown in Figs. 4a–c and 5a–c. This phenomenon is basically consistent with the variation characteristics of annual mean temperature in the Greater Bay Area under the background of global warming. This demonstrates that GHGs significantly affect the annual mean and extreme temperature in the Greater Bay Area. In summary, based on the above assessment, although there are a few slight systematic biases in annual mean SAT, annual T90 and T10 between the simulation and observation in some areas within this region, the WRF model can be considered capable of providing reasonable dynamically downscaling high-resolution climate simulations in the Greater Bay Area.

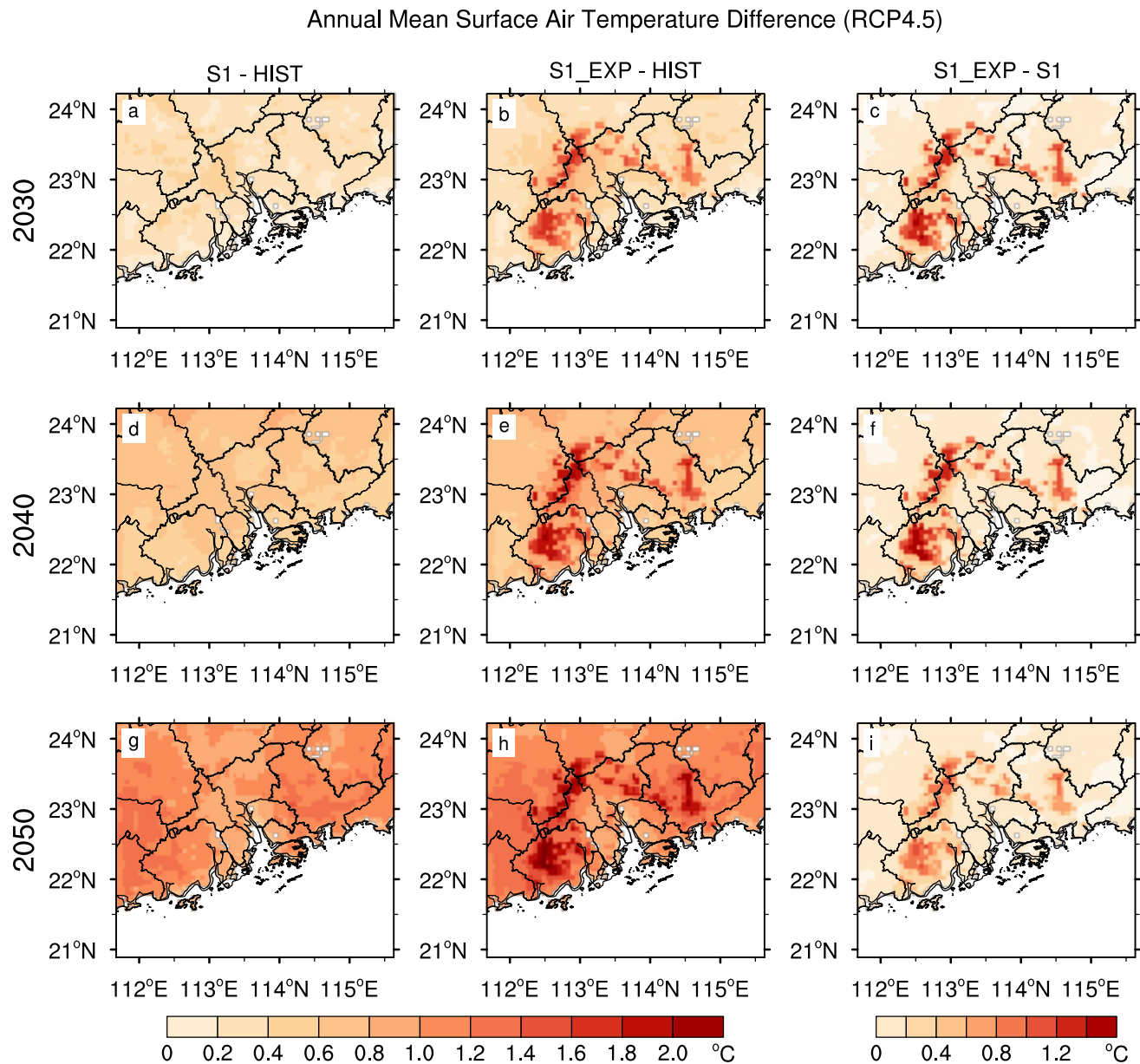


Fig. 7 Changes of annual mean surface air temperature in different forcing experiments (S1 and S1_EXP) under the RCP4.5 scenario. The left column is the change of surface air temperature in the S1 experiment, the middle column is the change in the S1_EXP, and the

right column is the difference between S1 and S1_EXP. The diagrams in (a–i) are for a–c the year of 2030, d–f the year of 2040, and g–i the year of 2050, respectively

3.2 Effects of GHGs concentration and urbanization on future temperature

3.2.1 Under the RCP4.5 scenario

As mentioned above, the GHGs forcing has a significant impact on temperature referring to the IPCC reports (IPCC AR4, 2007; IPCC AR5, 2013; IPCC AR6, 2021).

Urbanization can alter and influence the exchanges of substance and energy between urban surface and lower atmosphere, and in turn exert a great impact on the future temperature on urban local scale. However, how can we qualitatively and quantitatively distinguish the contributions of urbanization forcing (LULC change) from GHGs forcing on future temperature? In this section, based on the simulations of three numerical experiments (HIST, S1 and

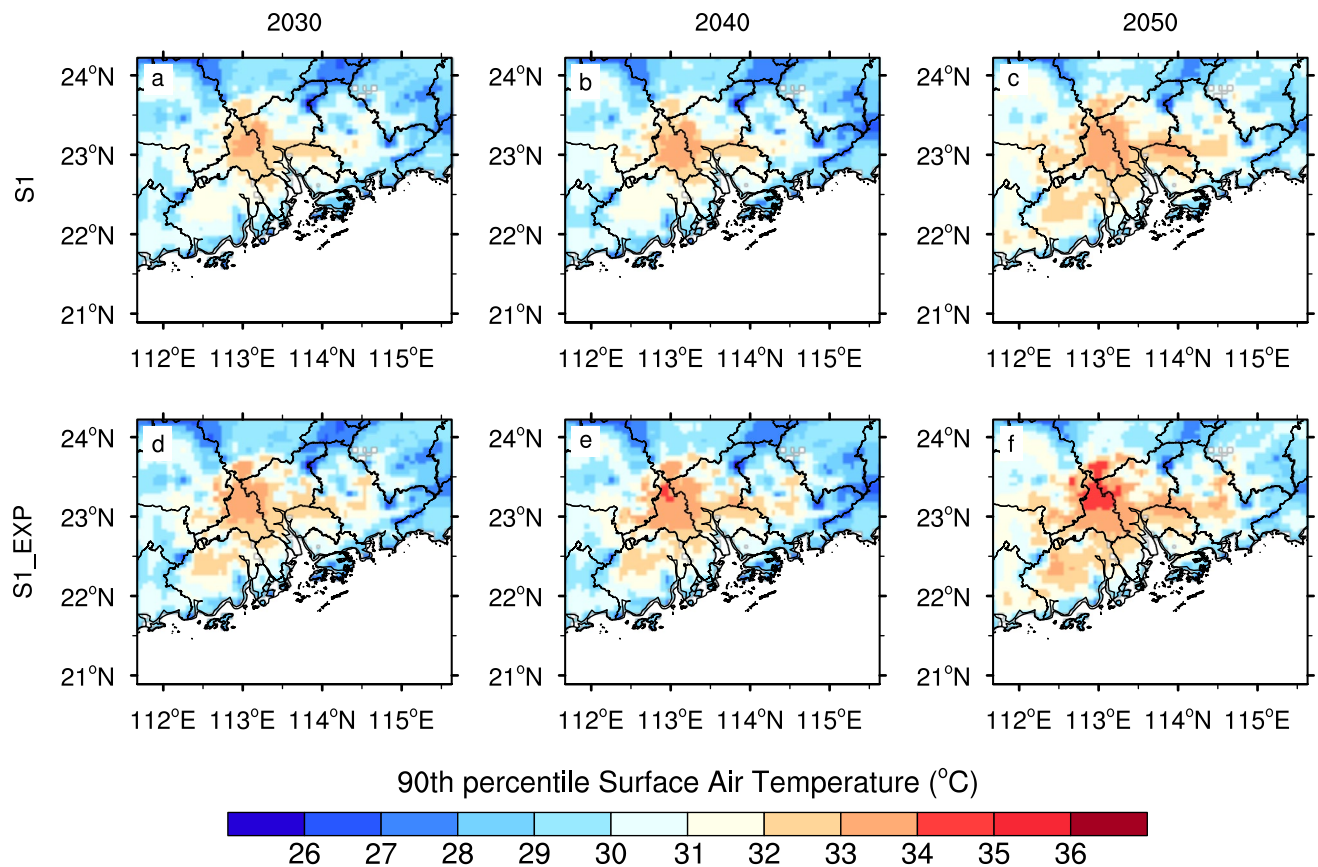


Fig. 8 Same as Fig. 6, but for the T90

S1_EXP, Table 3) under RCP4.5 scenario, the qualitative and quantitative contributions of LULC change induced by urbanization and GHGs concentration on future annual mean SAT, annual T90 and T10 are investigated in the Greater Bay Area under three different future climate scenarios (2030, 2040 and 2050), respectively.

Figure 6 shows the evolution characteristics of future annual mean SAT under the RCP4.5 forcing run scenario whether or not with urban expansion in the Greater Bay Area. Under the unexpanded urban scenario (Fig. 6a–c), the annual mean SAT will increase with the continuous increase of GHGs concentration in the whole region, especially in and around the urban areas of the Pearl River Delta Region. The area of relative high temperature (SAT > 23 °C) will also increase with the increase of GHGs concentration. This phenomenon is more obvious in the regional difference of SAT between S1 and HIST experiment, as shown in the left column of Fig. 7. By 2050, the annual mean SAT will rise by 1.4 °C in most of the Greater Bay Area from S1 simulation (Fig. 7g). Similar results can be found in the urbanization

expanded scenario (S1_EXP), as shown in Fig. 6d–f and the middle column of Fig. 7. By 2050, the annual mean SAT will rise by 1.4 °C in most of this region (Fig. 7g), but by almost 1.8 °C in the expanded urban area (Fig. 7h). That means the GHGs is the dominate factor for controlling the annual mean temperature evolution in the Greater Bay Area. The expanded urban area has slight positive contribution to the annual mean SAT for the whole region. Compared the expanded urban scenario with the unexpanded scenario, the expanded urban area has slight positive effects on the annual mean SAT of unchanged area on regional scale, but the annual mean SAT will obviously increase in the area where the underlying surface has been changed from rural to urban, reaching more than 1.0 °C, as shown in the right column of Fig. 7.

For extreme high and low temperature, the thresholds for annual T90 and T10 will also increase with the increase of GHGs concentration in the Greater Bay Area (Figs. 8a–c and 9a–c). Higher threshold and larger coverage area of T90

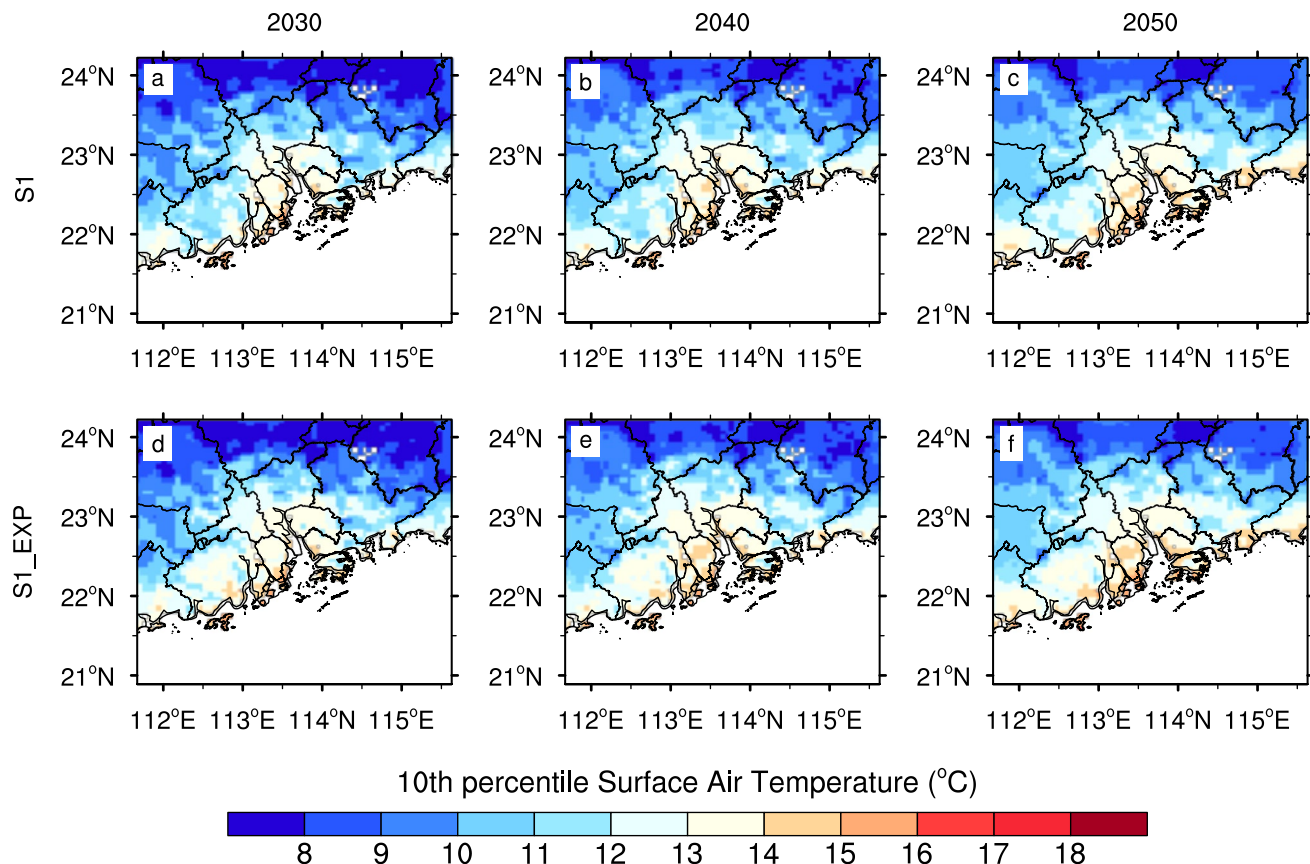


Fig. 9 Same as Fig. 6, but for the T10

and T10 will appear in the Pearl River Delta Region in the next 10–30 years. This phenomenon is more obvious and serious in the expanded urban area under the expanded urban scenario (S1_EXP) than that under the unexpanded urban scenario (S1), as shown in Figs. 8d–f and 9d–f. Same results could be found from the differences of extreme temperature between the S1 and S1_EXP simulations and historical simulations (Figs. 10 and 11). By 2050, under the expanded urban scenario, the threshold of T90 will be over 34 °C, and that of T10 will exceed 15 °C in some area of the Greater Bay Area. On the regional scale, same as the annual mean SAT, the GHGs is also the key factor for controlling extreme temperature in this region, and the expanded urban area will mainly affect the area where the underlying surface type has changed from rural to urban (the right columns of Figs. 10 and 11). From rural to urban, the biophysical properties of original underlying surface have changed, and in turn alter the surface energy redistribution and modulate the temperature. All these results indicate that the rapid development of urbanization in the Greater Bay Area has relatively

insignificant effect on temperature for the whole region during the next 10–30 years on regional scale, and the GHGs concentration is the key factor of dominating the regional annual mean SAT, annual T90 and T10. In another word, on the regional scale, large-scale atmospheric circulation is still more important than LULC change induced by urbanization for the future climate in the Greater Bay Area.

How about the contributions of LULC change induced by urbanization to mean and extreme temperature on urban local scale under different future climate scenarios? Fig. 9 shows the changes of annual mean SAT in different forcing experiments (S1 and S1_EXP) under RCP4.5 different future climate scenarios. The differences between the S1 and S1_EXP simulations represent the contribution of expanded urban area to temperature under different future climate scenario, as shown in the right column of Fig. 7. On local urban scale, the annual mean SAT will increase in the expanded urban area under different future climate scenarios. As shown in Table 6, the regional-averaged annual mean SAT of urban

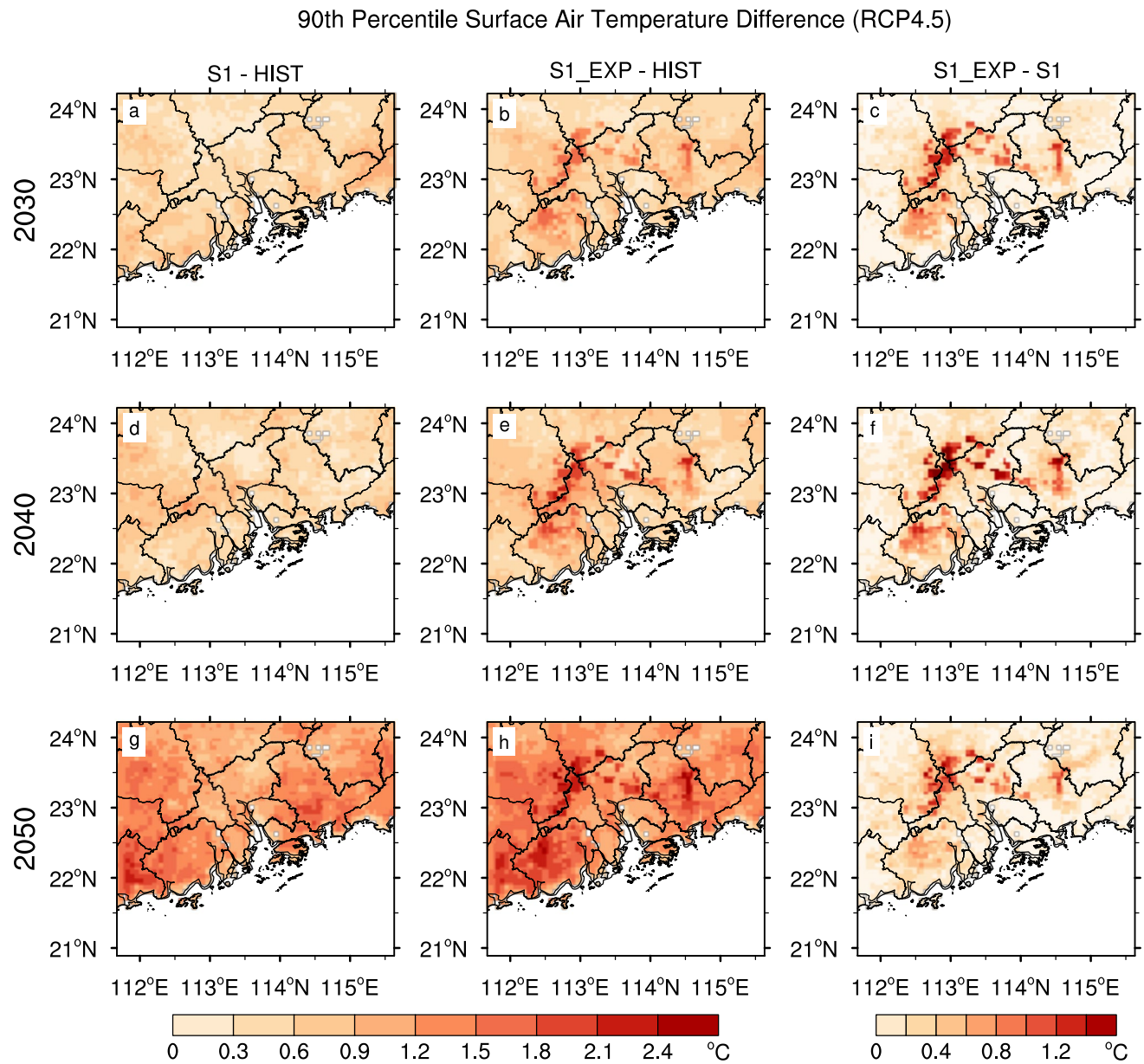


Fig. 10 Same as Fig. 7, but for the T90

area in the Great Bay Area are calculated to quantify the contributions of LULC change by urbanization and GHGs concentration to future annual mean SAT of the urban area. The regional-averaged annual mean SAT of urban area will increase 0.51 °C (2030), 0.83 °C (2040) and 1.26 °C (2050) under RCP4.5 different future climate scenarios resulting from the combined contributions of urbanization and GHGs forcing. Changes of the regional-averaged annual mean SAT due to GHGs forcing are 0.33 °C (2030), 0.66 °C (2040) and

1.12 °C (2050) in the urban area, LULC change by urbanization increases the SAT by 0.18 °C (2030), 0.17 °C (2040) and 0.14 °C (2050). That means GHGs concentration has relative significant impact on the regional-averaged annual mean SAT of urban area. Same as the annual mean SAT of urban area, based on the combined effects of GHGs concentration and urbanization, the regional-averaged annual T90 (T10) of urban area will increase 0.62 °C (0.24 °C), 0.72 °C (0.62 °C) and 1.39 °C (0.89 °C) in the year of 2030, 2040

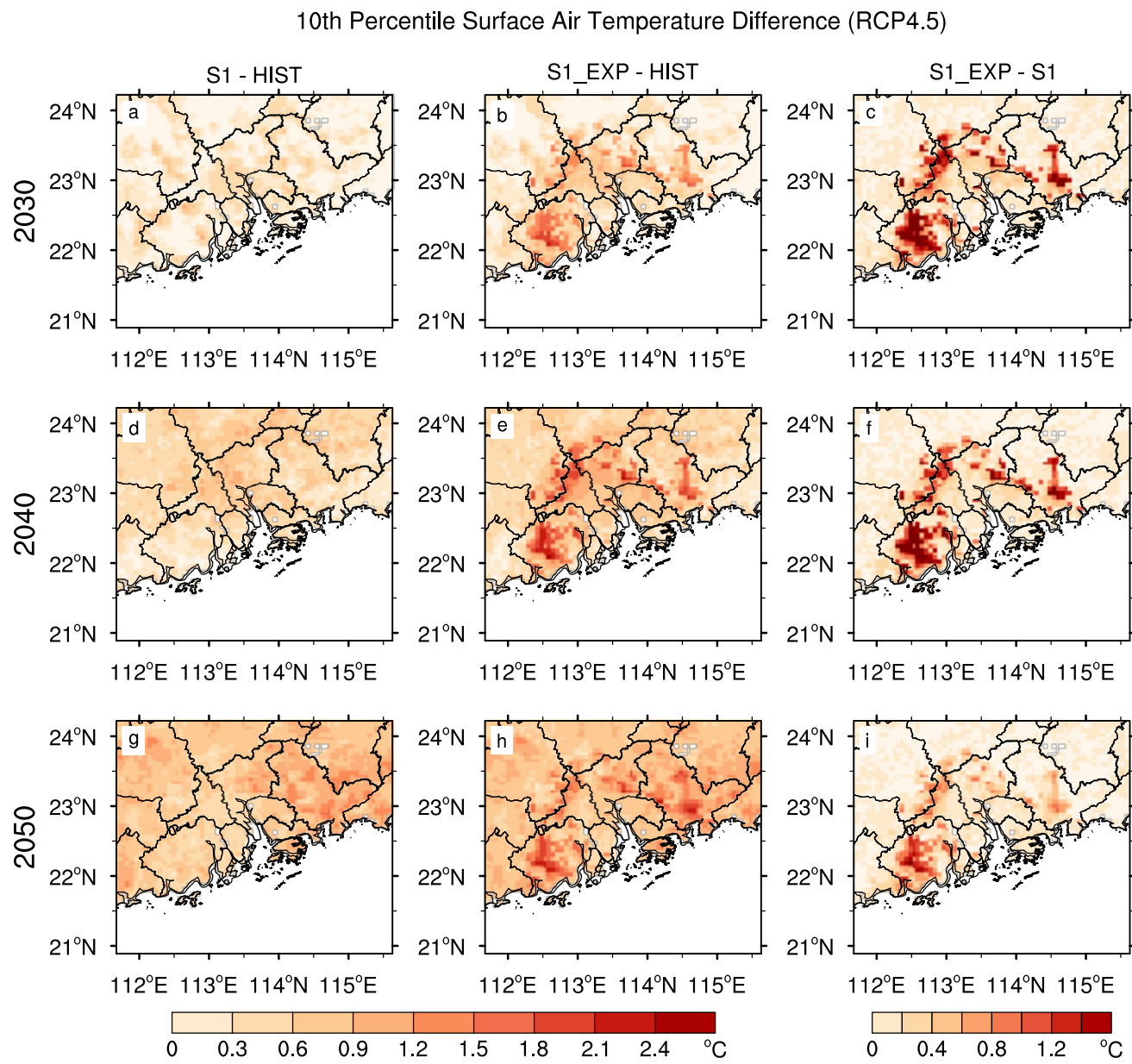


Fig. 11 Same as Fig. 7, but for the T10

Table 6 Statistical analysis of surface air temperature of urban area at different climate scenarios under the RCP4.5 and urbanization in the future over the Guangdong-Hong Kong-Macao Greater Bay Area (unit: °C)

| Different scenarios | S1 minus HIST | | | S1_EXP minus HIST | | | S1_EXP minus S1 | | |
|---------------------|---------------|------|------|-------------------|------|------|-----------------|------|------|
| | 2030 | 2040 | 2050 | 2030 | 2040 | 2050 | 2030 | 2040 | 2050 |
| Mean SAT | 0.33 | 0.66 | 1.12 | 0.51 | 0.83 | 1.26 | 0.18 | 0.17 | 0.14 |
| T90 | 0.50 | 0.54 | 1.25 | 0.62 | 0.72 | 1.39 | 0.12 | 0.18 | 0.14 |
| T10 | 0.05 | 0.43 | 0.78 | 0.24 | 0.62 | 0.89 | 0.19 | 0.19 | 0.11 |

The year of 2030, 2040 and 2050 represents different climate scenarios under the RCP4.5 scenario in the future world

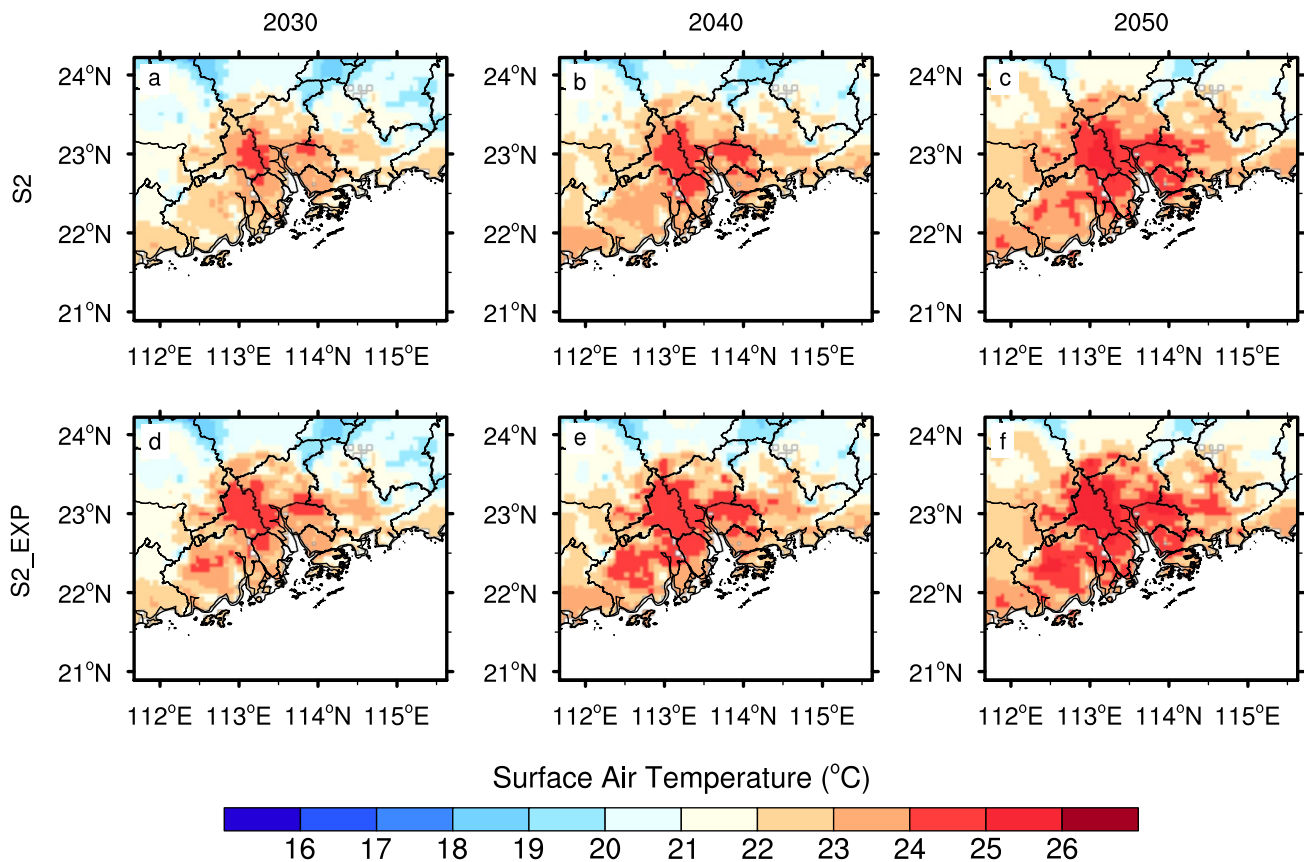


Fig. 12 Same as Fig. 6, but for under the RCP8.5 scenario

and 2050, respectively. Contributions of GHGs concentration to annual T90 (T10) are 0.50 °C (0.05 °C), 0.54 °C (0.43 °C) and 1.25 °C (0.78 °C), and contributions of urbanization are 0.12 °C (0.19 °C), 0.18 °C (0.19 °C) and 0.14 °C (0.11 °C) in the year of 2030, 2040 and 2050, respectively. All of these indicate that the GHGs contribution is also the key factor of dominating the extreme high- and low-temperature on the local urban scale, while the urbanization effect is second one. The higher thresholds of T90 and T10 will appear with the increase of GHGs concentration, especially for the T10. We also compared the regional-averaged annual mean SAT, annual T90 and T10 of the urban area with those of the non-urban area under different future climate scenarios, as shown in the left column of Fig. 18. In the future, temperature of the urban area will be higher than that in the non-urban area, and both of them will increase with the increase of GHGs concentration, especially for the T10. More GHGs in atmosphere, higher temperature in urban area.

3.2.2 Under the RCP8.5 scenario

The RCP8.5 scenario is a high emission path, and GHGs concentration will continue to rise before 2100. In this section, we present the future temperature projection in the Greater Bay Area under RCP8.5 scenario. Same as under the RCP4.5 scenario, on the regional scale, the annual mean SAT, annual T90 and T10 will increase with the increase of GHGs concentration under RCP8.5 scenario in the future, as shown in Figs. 12, 13 and 14. Compared with under RCP4.5 scenario (Fig. 6a–c), the annual mean SAT will be much higher in the region, and the area of SAT greater than 23 °C will be much larger (Fig. 12a–c). This phenomenon becomes more obvious when the urban area has expanded (Fig. 12d–f and the middle column of Fig. 15). By 2050, the annual mean SAT will rise by 1.8 °C in most of this region (Fig. 15g), but by almost 2.0 °C in the expanded urban area (Fig. 15h). For the extreme high- and low- temperature, the

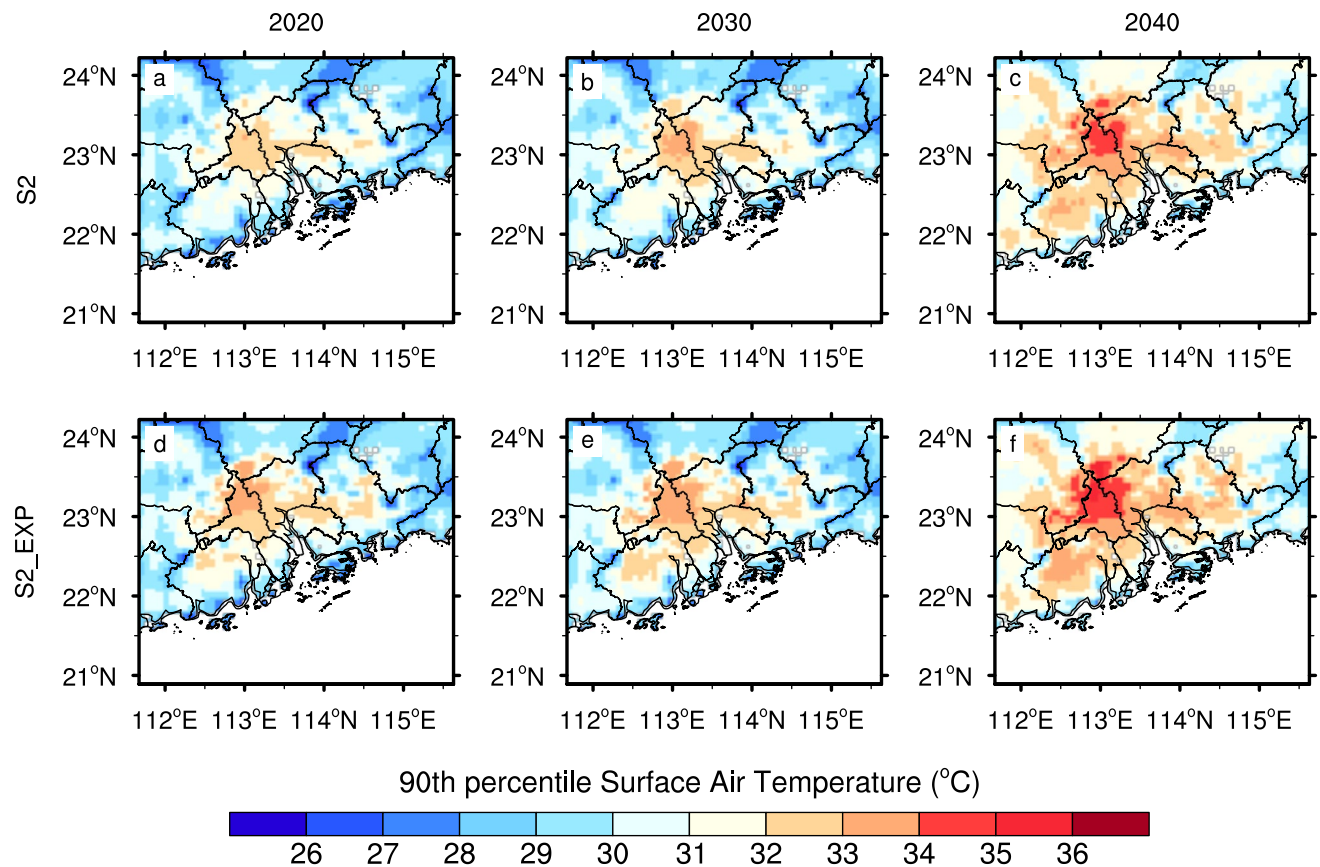


Fig. 13 Same as Fig. 8, but for under the RCP8.5 scenario

thresholds and coverage areas of annual T90 and T10 will also rise and expand under RCP8.5 scenarios (Fig. 13a–c and 14a–c). The warming and expansion phenomenon are more obvious and serious in the expanded urban scenario (S2_EXP) than that in the non-expanded scenario (S2), as shown in Figs. 13d–f and 14d–f. Same results could be found in the difference of annual mean SAT, annual T90 and T10 between the future and historical scenarios (the left and middle columns of Figs. 15, 16 and 17). By 2050, higher threshold and larger coverage area of T90 and T10 will appear in the Pearl River Delta Region, especially for the T10 (Fig. 14f). Under the expanded urban scenario, the threshold of T90 will be over 35 °C, and that of T10 will exceed 16 °C in some area of the Greater Bay Area in 2050. On the regional scale, same as under the RCP4.5 scenario, the GHGs is the main dominate factor for controlling annual mean SAT and extreme temperature in this region, and the expanded urban area mainly affect the area where the original underlying surface type has changed to urban (the right columns of Figs. 15, 16, 17).

On local urban scale, as shown in Table 7, the regional-averaged annual mean SAT of urban area will increase

0.73 °C (2030), 1.17 °C (2040) and 1.74 °C (2050) under RCP8.5 different future climate scenarios resulting from the combined contributions of urbanization and GHGs forcing. Changes of the regional-averaged annual mean SAT induced by GHGs forcing are 0.53 °C (2030), 1.00 °C (2040) and 1.58 °C (2050) in the urban area, and urbanization increases the SAT by 0.20 °C (2030), 0.17 °C (2040) and 0.16 °C (2050), respectively. Based on the combined effects of GHGs concentration and urbanization, the regional-averaged annual T90 (T10) of urban area will increase 0.69 °C (0.96 °C), 0.87 °C (1.60 °C) and 2.08 °C (1.92 °C) in the year of 2030, 2040 and 2050, respectively. Contributions of GHGs concentration to annual T90 (T10) are 0.46 °C (0.77 °C), 0.66 °C (1.50 °C) and 1.93 °C (1.73 °C), and contributions of urbanization are 0.23 °C (0.19 °C), 0.21 °C (0.10 °C) and 0.15 °C (0.19 °C) in the year of 2030, 2040 and 2050, respectively. All of these indicate that the GHGs

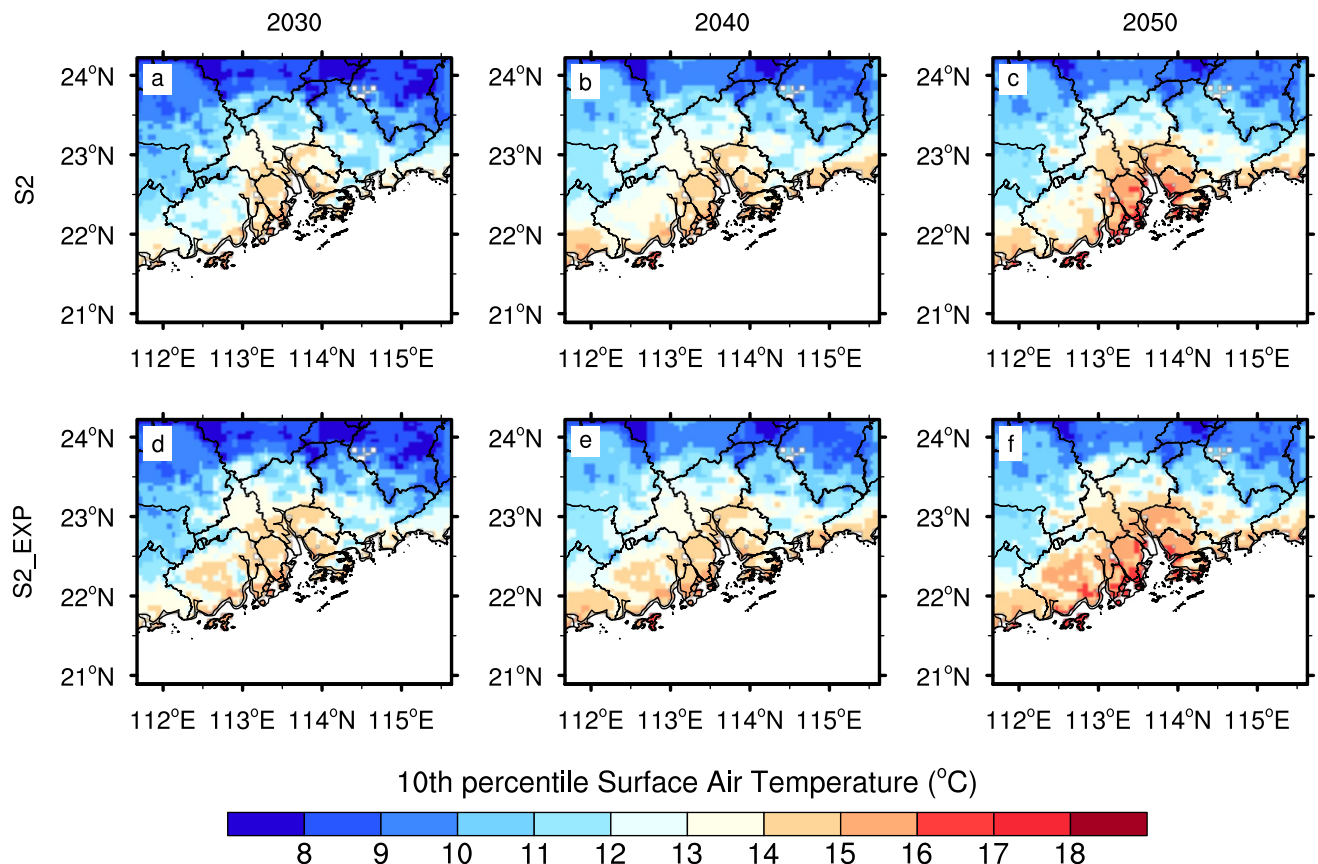


Fig. 14 Same as Fig. 9, but for under the RCP8.5 scenario

concentration has relative significant impact on the regional-averaged mean and extreme temperature of urban area. The extreme temperature is much more sensitively to GHGs concentration under RCP8.5 scenario than that under RCP4.5 scenario. The impact of urbanization is local and the second one. Temperature of the urban area will be higher than that in the non-urban area, and both of them will increase with the increase of GHGs concentration, especially for the T10, as shown in the right column of Fig. 18. In summary, the GHGs is the dominate factor for controlling the annual mean and extreme temperature evolution in the next 10–30 years, the expanded urban area has slight positive contribution to the temperature and its impact is local in the Greater Bay Area.

4 Conclusions and discussion

In this study, we used the WRF model to investigate the relative contributions (qualitative and quantitative) of GHGs concentration and land use/cover change induced by urbanization on future annual mean and extreme high- and low- temperatures in the Guangdong-Hong Kong-Macao

Greater Bay Area in China under RCP4.5&8.5 scenarios. Under the RCP4.5 scenario, the regional-averaged annual mean SAT of urban area is projected to increase 0.51 °C (2030), 0.83 °C (2040) and 1.26 °C (2050) under different future climate scenarios resulting from the combined contributions of urbanization and GHGs forcing. The regional-averaged annual mean SAT of urban area changed by the GHGs forcing will increase 0.33 °C (2030), 0.66 °C (2040) and 1.12 °C (2050), the urbanization forcing will increase the annual mean SAT by 0.18 °C (2030), 0.17 °C (2040) and 0.14 °C (2050), respectively. That means GHGs concentration has significant impact on the regional-averaged annual mean SAT of urban area. The regional-averaged annual T90 (T10) of urban area will increase 0.62 °C (0.24 °C), 0.72 °C (0.62 °C) and 1.39 °C (0.89 °C) in the year of 2030, 2040 and 2050 due to the combined effects of GHGs concentration and urbanization. Contributions of GHGs concentration to annual T90 (T10) are 0.50 °C (0.05 °C), 0.54 °C (0.43 °C) and 1.25 °C (0.78 °C), and contributions of urbanization are 0.12 °C (0.19 °C), 0.18 °C (0.19 °C) and 0.14 °C (0.11 °C) in the year of 2030, 2040 and 2050. For the RCP8.5 scenarios, the regional-averaged annual mean SAT of urban area will increase 0.73 °C (2030), 1.17 °C (2040) and 1.74 °C

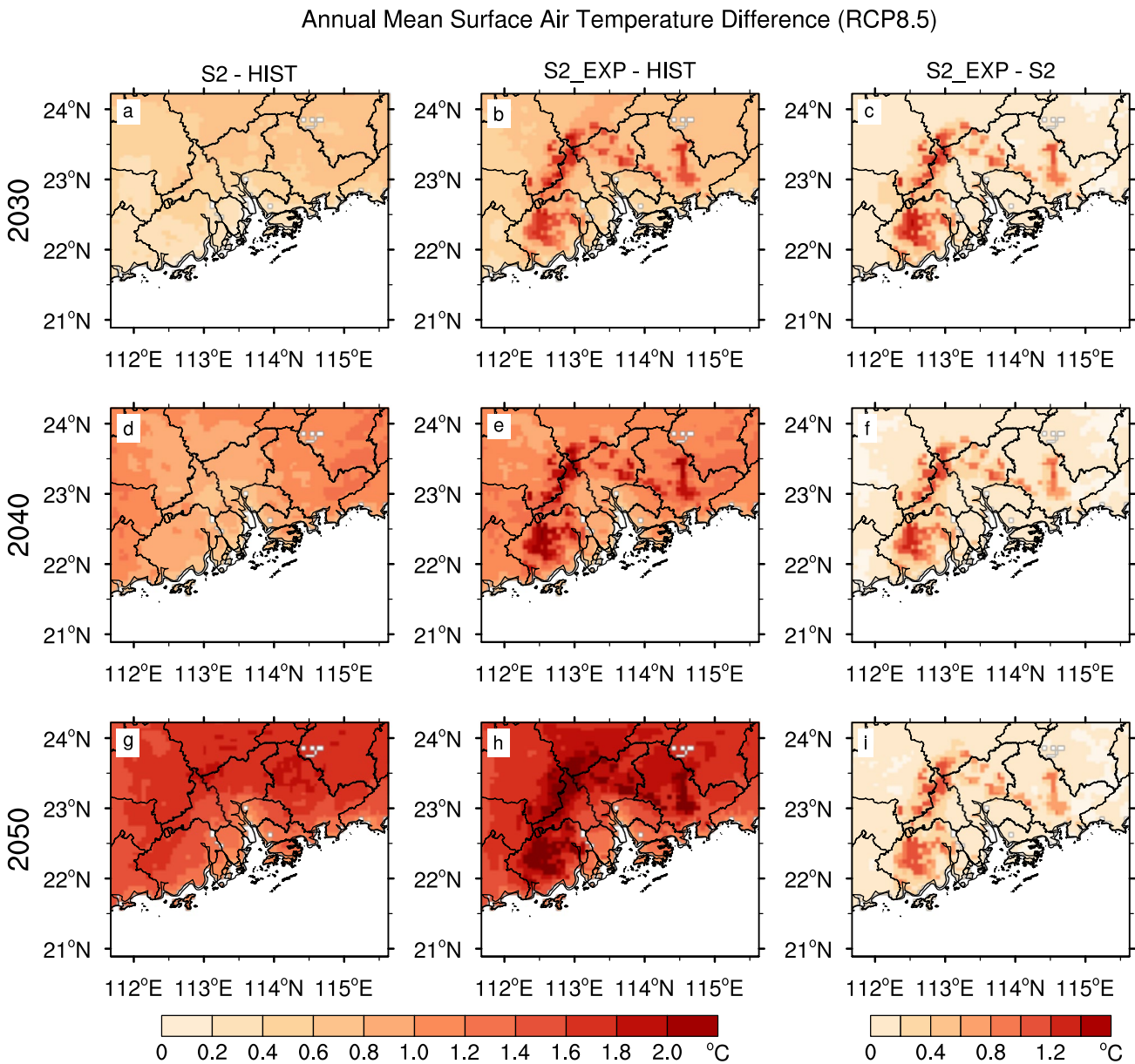


Fig. 15 Same as Fig. 7, but for under the RCP8.5 scenario

(2050) in the future resulting from the combined contributions of urbanization and GHGs. Changes of the regional-averaged annual mean SAT induced by GHGs forcing are 0.53 °C (2030), 1.00 °C (2040) and 1.58 °C (2050) in the urban area, and urbanization increases the SAT by 0.20 °C (2030), 0.17 °C (2040) and 0.16 °C (2050), respectively. Based on the combined effects of GHGs concentration and urbanization, the regional-averaged annual T90 (T10) of urban area will increase 0.69 °C (0.96 °C), 0.87 °C (1.60 °C) and 2.08 °C (1.92 °C) in the year of 2030, 2040 and 2050, respectively. Contributions of GHGs concentration to annual

T90 (T10) are 0.46 °C (0.77 °C), 0.66 °C (1.50 °C) and 1.93 °C (1.73 °C), and contributions of urbanization are 0.23 °C (0.19 °C), 0.21 °C (0.10 °C) and 0.15 °C (0.19 °C) in the year of 2030, 2040 and 2050, respectively.

On the regional scale, the development of urbanization in the Greater Bay Area has relative slight effect on the SAT in the next 10–30 years, the GHGs concentration is the key factor for dominating the SAT. Large-scale atmospheric circulation is still the main dominating factor for the future mean and extreme temperature of the Greater Bay Area. On the urban local scale, the LULC change in urban

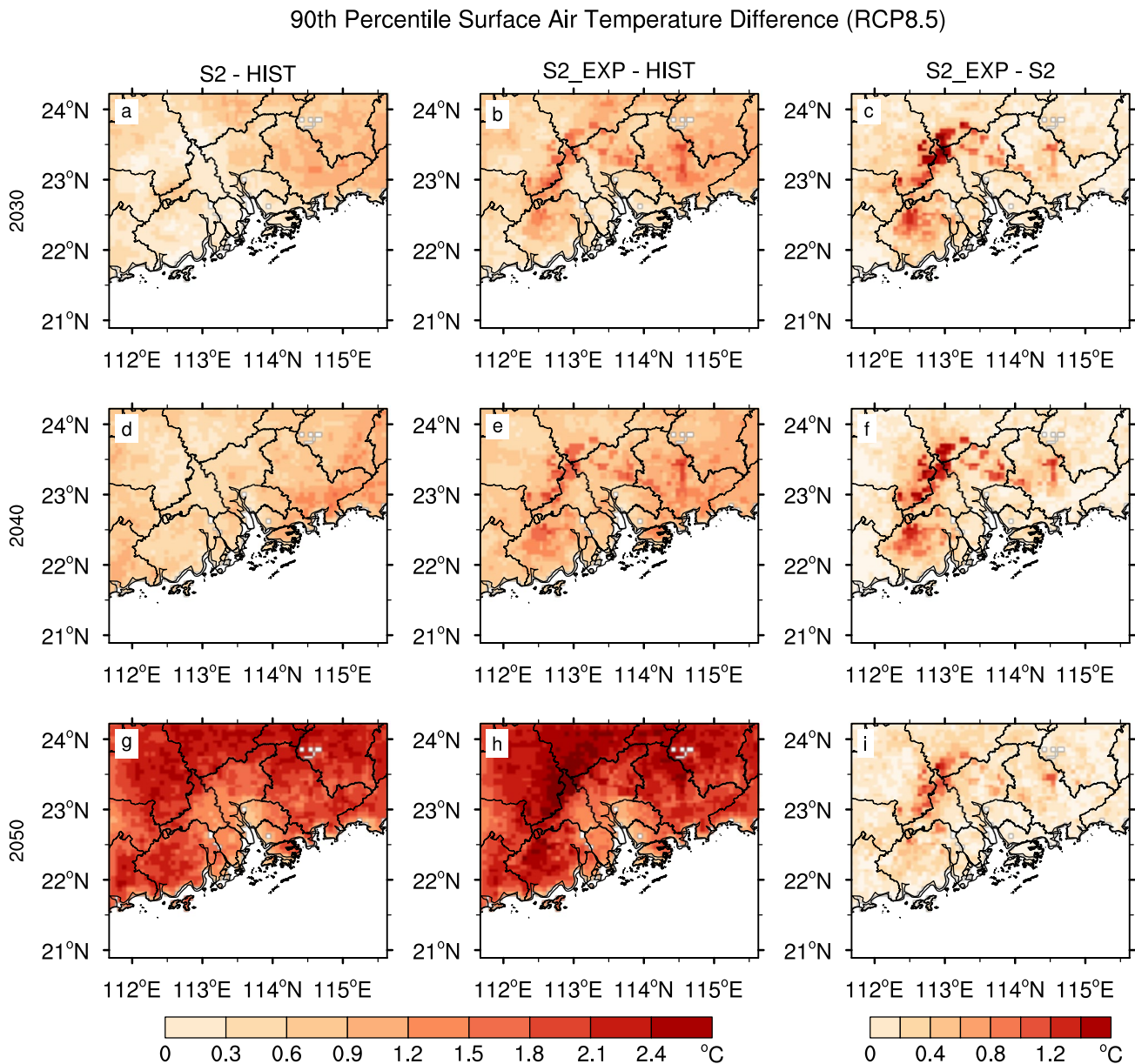


Fig. 16 Same as Fig. 10, but for under the RCP8.5 scenario

area has an obvious effect on the local temperature of the city. Moreover, the extreme temperature is much more sensitively to GHGs concentration under RCP8.5 scenario than that under RCP4.5 scenario. Temperature of the urban area will be higher than that in the non-urban area, and both of them will increase with the increase of GHGs concentration, especially for the T10.

In this study, we only focused on the biogeophysical effects of urbanization on annual mean and extreme temperature in the Greater Bay Area. There are also some

limitations in this study, such as the effects of the urban expanded scenario and the urban morphology. Anthropogenic heat flux (Ichinose et al. 1999; Sailor and Lu 2004; Flanner 2009; Yang et al. 2012; Feng et al. 2014), urban aerosol (Kaufmann et al. 2007; Sun et al. 2021; Yang et al. 2021) and the interaction between urban aerosol and urban heat island (Yang et al. 2021) can also affect the regional and local weather and climate during urbanization processes. All of these should be considered in the Greater Bay Area in the future work.

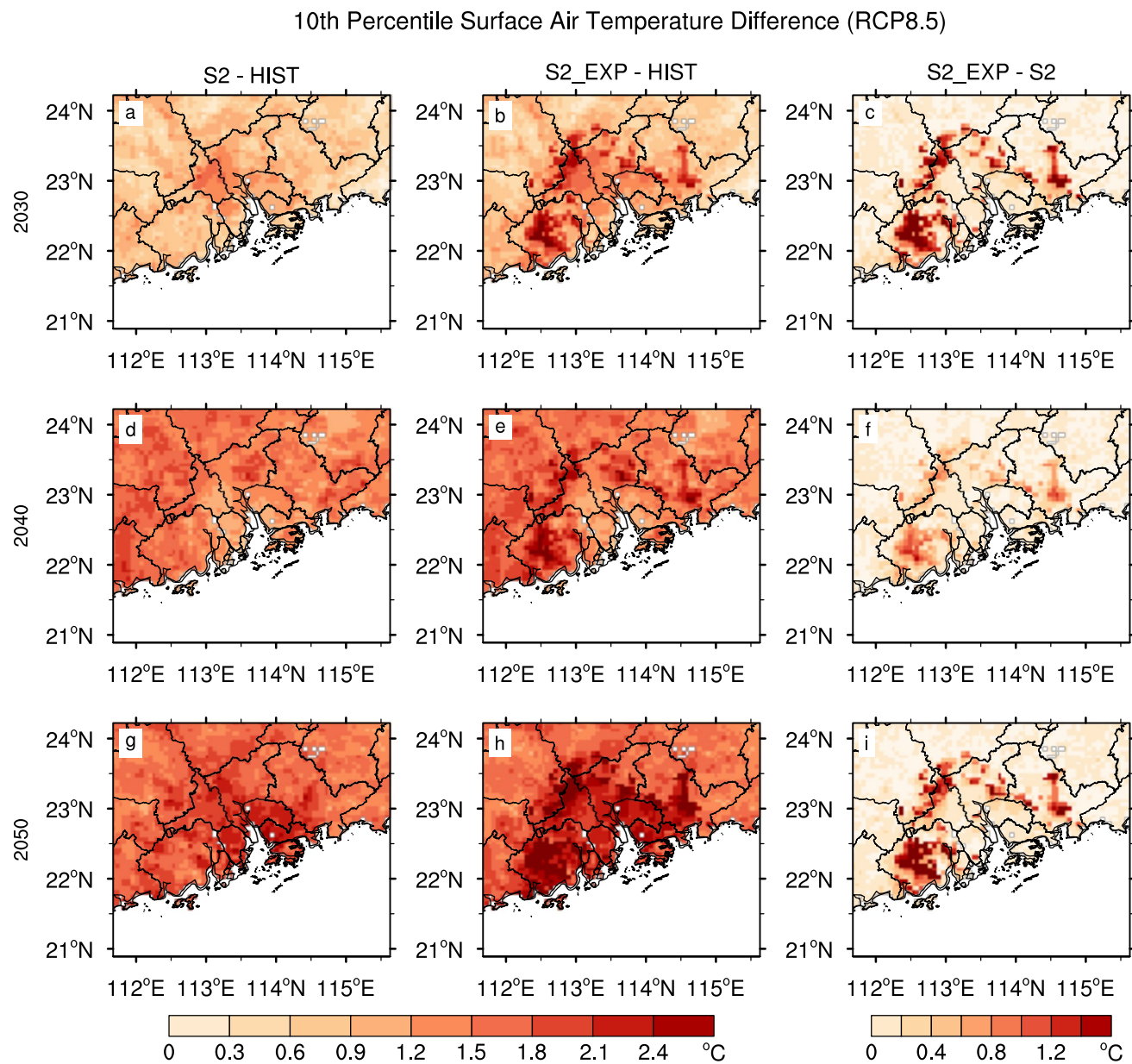


Fig. 17 Same as Fig. 11, but for under the RCP8.5 scenario

Table 7 Same as Table 6, but for the RCP8.5 scenario

| Different scenarios | S2 minus HIST | | | S2_EXP minus HIST | | | S2_EXP minus S2 | | |
|---------------------|---------------|------|------|-------------------|------|------|-----------------|------|------|
| | 2030 | 2040 | 2050 | 2030 | 2040 | 2050 | 2030 | 2040 | 2050 |
| Mean SAT | 0.53 | 1.00 | 1.58 | 0.73 | 1.17 | 1.74 | 0.20 | 0.17 | 0.16 |
| T90 | 0.46 | 0.66 | 1.93 | 0.69 | 0.87 | 2.08 | 0.23 | 0.21 | 0.15 |
| T10 | 0.77 | 1.50 | 1.73 | 0.96 | 1.60 | 1.92 | 0.19 | 0.10 | 0.19 |

The year of 2030, 2040 and 2050 represents different climate scenarios under the RCP8.5 scenario in the future world

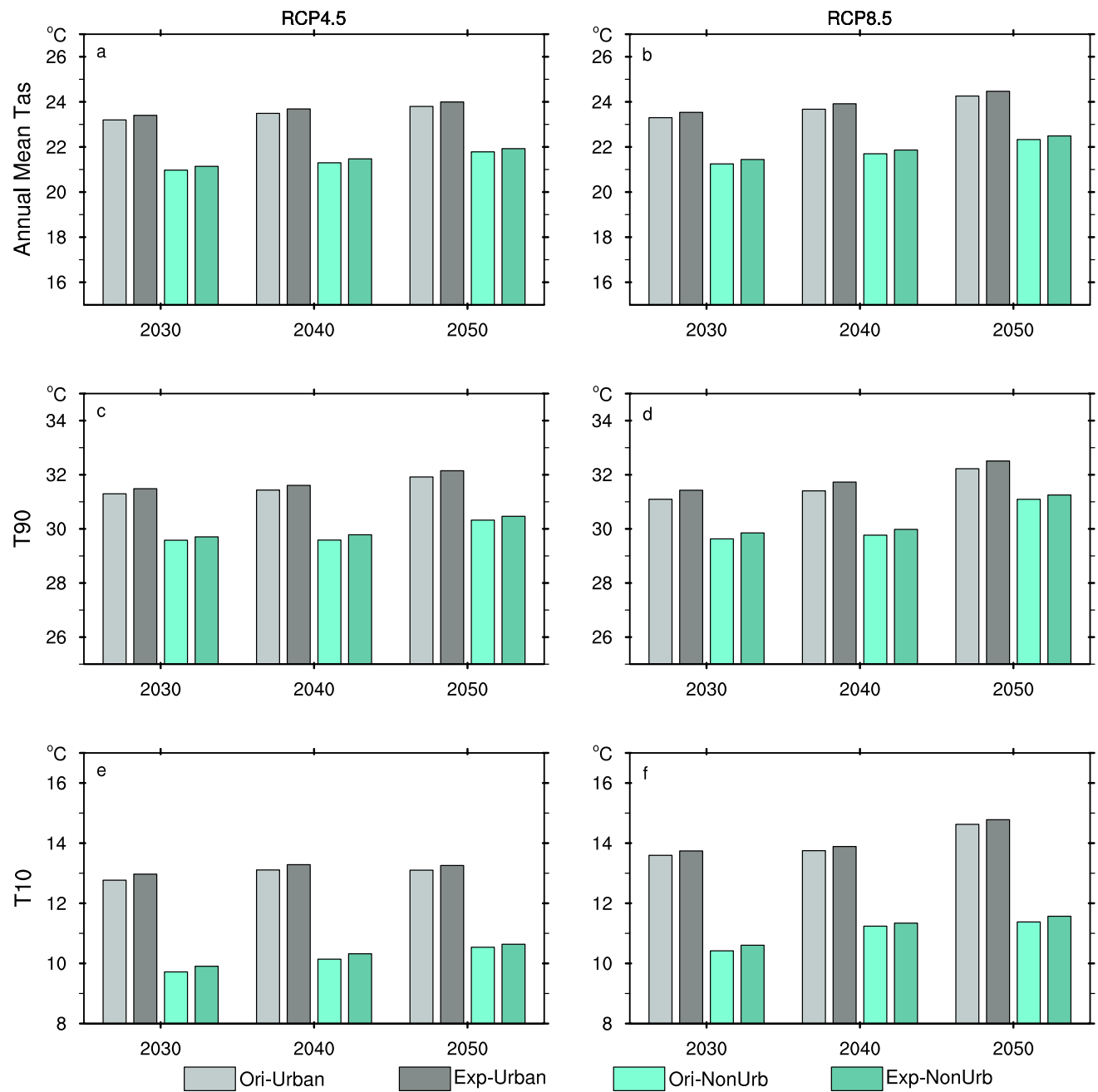


Fig. 18 Comparisons of the regional-averaged annual mean SAT, annual T90 and T10 between urban area and non-urban area in three different experiments for different future climate scenarios under the RCP4.5&8.5 scenarios. The left column is the result under RCP4.5,

and the right column is the result under RCP8.5. Ori-Urban and Ori-NonUrb denote the experiments only with GHGs, EXP-Urban and EXP-NonUrb denote the experiments with GHGs and urbanized expanded land cover condition

Acknowledgements This research is jointly supported by the National Natural Science Foundation of China (42005114 and 41775015), the Project funded by China Postdoctoral Science Foundation (2019M663206), the Project supported Innovation Group Project of Southern Marine Science and Engineering Guangdong Laboratory (Zhuhai) (311021009), the Guangdong Major Project of Basic and Applied Basic Research (2020B0301030004), and the Fundamental Research Funds for the Central Universities, Sun Yat-sen University (2021qntd29 and 20lgpy28). The Climatic Research Unit gridded Time

Series (CRU TS) dataset version 4 produced by the UK's National Centre for Atmospheric Science (NCAS) at the University of East Anglia's Climatic Research Unit (CRU) can be obtain from <https://crudata.uea.ac.uk/cru/data/hrg/>. The NCAR CESM Global Bias-Corrected CMIP5 Output to Support WRF/MPAS Research dataset can be obtain from the Computational and Information Systems Laboratory (CISL) Research Data Archive at NCAR <https://rda.ucar.edu/datasets/ds316.1/>. We are very grateful to the editor and anonymous reviewers for their careful

review and valuable comments, which led to substantial improvement of this work.

References

- Argüeso D, Evans J, Fita L, Bormann K (2014) Temperature response to future urbanization and climate change. *Clim Dyn* 42:2183–2199. <https://doi.org/10.1007/s00382-013-1789-6>
- Bassett R, Young PJ, Blair GS, Cai XM, Chapman L (2020) Urbanisation's contribution to climate warming in Great Britain. *Environ Res Lett* 15:114014. <https://doi.org/10.1088/1748-9326/abbb51>
- Bruyère CL, Done JM, Holland GJ, Fredrick S (2014) Bias corrections of global models for regional climate simulations of high-impact weather. *Clim Dyn* 43:1847–1856. <https://doi.org/10.1007/s00382-013-2011-6>
- Chen L, Frauenfeld OW (2014a) Surface air temperature changes over the 20th and 21st centuries in China simulated by 20 CMIP5 models. *J Climate* 27:3920–3937. <https://doi.org/10.1175/JCLI-D-13-00465.1>
- Chen L, Frauenfeld OW (2014b) A comprehensive evaluation of precipitation simulations over China based on CMIP5 multimodel ensemble projections. *J Geophys Res Atmos* 119:5767–5786. <https://doi.org/10.1002/2013JD021190>
- Chen L, Frauenfeld OW (2016) Impacts of urbanization on future climate in China. *Clim Dyn* 47:345–357. <https://doi.org/10.1007/s00382-015-2840-6>
- Chen S-H, Sun W-Y (2002) A one-dimensional time dependent cloud model. *J Meteorol Soc Jpn Ser II* 80(1):99–118. <https://doi.org/10.2151/jmsj.80.99>
- Chen F, Kusaka H, Bornstein R, Ching J, Grimmond CSB, Grossmann-Clarke S, Loridan T, Manning KW, Martilli A, Miao S, Sailor D, Salamanca FP, Taha H, Tewari M, Wang X, Wyszogrodzki AA, Zhang C (2011) The integrated WRF/urban modelling system: development, evaluation, and applications to urban environmental problems. *Int J Climatol* 31:273–288. <https://doi.org/10.1002/joc.2158>
- Dee DP, Uppala SM, Simmons AJ, Berrisford P, Poli P, Kobayashi S, Andrae U, Balmaseda MA, Balsamo G, Bauer P, Bechtold P, Beljaars ACM, van de Berg L, Bidlot J, Bormann N, Delsol C, Dragani R, Fuentes M, Geer AJ, Haimberger L, Healy SB, Hersbach H, Hölm EV, Isaksen L, Källberg P, Köhler M, Matricardi M, McNally AP, Monge-Sanz BM, Morcrette J-J, Park B-K, Peubey C, de Rosnay P, Tavolato C, Thépaut J-N, Vitart F (2011) The ERA-Interim reanalysis: configuration and performance of the data assimilation system. *Q J R Meteorol Soc* 137:553–597. <https://doi.org/10.1002/qj.828>
- Di Vittorio AV, Chini LP, Bond-Lamberty B, Mao J, Shi X, Truesdale J, Craig A, Calvin K, Jones A, Collins WD, Edmonds J, Hurtt GC, Thornton P, Thomson A (2014) From land use to land cover: restoring the afforestation signal in a coupled integrated assessment—earth system model and the implications for CMIP5 RCP simulations. *Biogeosciences* 11:6435–6450. <https://doi.org/10.5194/bg-11-6435-2014>
- Feng JM, Wang YL, Ma ZG, Liu YH (2012) Simulating the regional impacts of urbanization and anthropogenic heat release on climate across China. *J Climate* 25:7187–7203. <https://doi.org/10.1175/JCLI-D-11-00333.1>
- Feng JM, Wang YL, Ma ZG (2013) Long-term simulation of large-scale urbanization effect on the East Asian monsoon. *Clim Change* 129:511–523. <https://doi.org/10.1007/s10584-013-0885-2>
- Feng JM, Wang J, Yan ZW (2014) Impact of anthropogenic heat release on regional climate in three vast urban agglomerations in China. *Adv Atmos Sci* 31:363–373. <https://doi.org/10.1007/s00376-013-3041-z>
- Flanner MG (2009) Integrating anthropogenic heat flux with global climate models. *Geophys Res Lett* 36:L02801. <https://doi.org/10.1029/2008GL036465>
- Gao XJ, Shi Y, Giorgi F (2011) A high resolution simulation of climate change over China. *Sci China Earth Sci* 54:462–472. <https://doi.org/10.1007/s11430-010-4035-7>
- Gao XJ, Shi Y, Zhang D, Giorgi F (2012) Climate change in China in the 21st century as simulated by a high resolution regional climate model. *Chin Sci Bull* 57:1188–1195. <https://doi.org/10.1007/s11434-011-4935-8>
- Gao ZB, Zhu JS, Guo Y, Luo N, F Y, Wang TT (2021) Impact of land surface processes on a record-breaking rainfall event on May 06–07, 2017, in Guangzhou, China. *J Geophys Res Atmos*. <https://doi.org/10.1029/2020JD032997>
- Gong P, Liang S, Carlton EJ, Jiang QW, Wu JY, Wang L, Remais JV (2012) Urbanisation and health in China. *Lancet* 379:843–852. [https://doi.org/10.1016/S0140-6736\(11\)61878-3](https://doi.org/10.1016/S0140-6736(11)61878-3)
- Han WC, Li ZQ, Wu F, Zhang YW, Guo JP, Su TN, Cribb M, Fan JW, Chen TM, Wei J, Lee S-S (2020) The mechanisms and seasonal differences of the impact of aerosols on daytime surface urban heat island effect. *Atmos Chem Phys* 20:6479–6493. <https://doi.org/10.5194/acp-20-6479-2020>
- Harris I, Osborn TJ, Jones P, Lister D (2020) Version 4 of the CRU TS monthly high-resolution gridded multivariate climate dataset. *Sci Data* 7:109. <https://doi.org/10.1038/s41597-020-0453-3>
- Hong S-Y, Noh Y, Dudhia J (2006) A new vertical diffusion package with an explicit treatment of entrainment processes. *Mon Weather Rev* 134:2318–2341. <https://doi.org/10.1175/MWR3199.1>
- Huang B, Hu XP, Fuglstad G-A, Zhou X, Zhao WX, Cherubini F (2020) Predominant regional biophysical cooling from recent land cover changes in Europe. *Nat Commun* 11:1066. <https://doi.org/10.1038/s41467-020-14890-0>
- Iacono MJ, Delamere JS, Mlawer EJ, Shephard MW, Clough SA, Collins WD (2008) Radiative forcing by long-lived greenhouse gases: calculations with the AER radiative transfer models. *J Geophys Res Atmos* 113:D13103. <https://doi.org/10.1029/2008JD009944>
- Lamichhane S, Shakya NM (2019a) Alteration of groundwater recharge areas due to land use/cover change in Kathmandu Valley, Nepal. *J Hydrol Reg Stud* 26:100635. <https://doi.org/10.1016/j.ejrh.2019.100635>
- Lamichhane S, Shakya NM (2019b) Integrated assessment of climate change and land use change impacts on hydrology in the Kathmandu Valley Watershed, Central Nepal. *Water* 11:1–17. <https://doi.org/10.3390/w11102059>
- Lamichhane S, Shakya NM (2020) Shallow aquifer groundwater dynamics due to land use/cover change in highly urbanized basin: the case of Kathmandu Valley. *J Hydrol Reg Stud* 30:100707. <https://doi.org/10.1016/j.ejrh.2020.100707>
- Ichinose T, Shimodozo K, Hanaki K (1999) Impact of anthropogenic heat on urban climate in Tokyo. *Atmos Environ* 33:3897–3909. [https://doi.org/10.1016/S1352-2310\(99\)00132-6](https://doi.org/10.1016/S1352-2310(99)00132-6)
- IPCC (2007) Contribution of Working Group I to the Fourth Assessment Report of the Intergovernmental Panel on Climate Change, 2007. Cambridge University Press, Cambridge
- IPCC (2013) Climate Change 2013: The Physical Science Basis. In: Stocker TF, Qin D, Plattner G-K et al (eds) Contribution of working group I to the Fifth Assessment Report of the Intergovernmental Panel on Climate Change. Cambridge University Press, Cambridge, p 1256
- IPCC (2021) Summary for policymakers. In: Masson-Delmotte V, Zhai P, Pirani A, Connors SL, Péan C, Berger S, Caud N, Chen Y, Goldfarb L, Gomis MI, Huang M, Leitzell K, Lonnoy E, Matthews JBR, Maycock TK, Waterfield T, Yeolekci O, Yu R, Zhou B (eds) Climate change 2021: the physical science basis. Contribution of working group I to the Sixth Assessment Report of the

- Intergovernmental Panel on Climate Change. Cambridge University Press, Cambridge
- Jiménez PA, Dudhia J, González-Rouco JF, Navarro J, Montávez JP, García-Bustamante E (2012) A revised scheme for the WRF surface layer formulation. *Mon Wea Rev* 140:898–918. <https://doi.org/10.1175/MWR-D-11-00056.1>
- Kain JS (2004) The Kain–Fritsch convective parameterization: an update. *J Appl Meteorol* 43:170–181. [https://doi.org/10.1175/1520-0450\(2004\)043%3c0170:TKCPAU%3e2.0.CO;2](https://doi.org/10.1175/1520-0450(2004)043%3c0170:TKCPAU%3e2.0.CO;2)
- Kaufmann RK, Seto KC, Schneider A, Liu ZT, Zhou LM, Wang WL (2007) Climate response to rapid urban growth: evidence of a human-induced precipitation deficit. *J Clim* 20:2299–2306. <https://doi.org/10.1175/JCLI4109.1>
- Knutti R, Sedlacek J (2013) Robustness and uncertainties in the new CMIP5 climate model projections. *Nat Climate Change* 3:369–373. <https://doi.org/10.1038/nclimate1716>
- Kong DD, Gu XH, Li JF, Ren GY, Liu JY (2020) Contributions of global warming and urbanization to the intensification of human-perceived heatwaves over China. *J Geophys Res Atmos.* <https://doi.org/10.1029/2019JD03217>
- Lejeune Q, Seneviratne SI, Davin EL (2017) Historical land-cover change impacts on climate: comparative assessment of LUCID and CMIP5 multimodel experiments. *J Clim* 30:1439–2145. <https://doi.org/10.1175/JCLI-D-16-0213.1>
- Liao WL, Liu XP, Li D, Luo M, Wang DG, Wang SJ, Baldwin J, Lin LJ, Li X, Feng KS, Hubacek K, Yang XC (2018) Stronger contributions of urbanization to heat wave trends in wet climates. *Geophys Res Lett.* <https://doi.org/10.1029/2018GL079679>
- Liu B, Xie ZH, Qin PH, Liu S, Li RC, Wang LH, Wang Y, Jia BH, Chen S, Xie JB, Shi CX (2021) Increases in anthropogenic heat release from energy consumption lead to more frequent extreme heat events in urban cities. *Adv Atmos Sci* 38:430–445. <https://doi.org/10.1007/s00376-020-0139-y>
- Mahmood R, Pielke RA, Hubbard KG, Niyogi D, Dirmeyer PA, McAlpine C, Carleton AM, Hale R, Gaméda S, Beltrán-Przekurat A, Baker B, McNider R, Legates DR, Shepherd M, Du J, Blanken PD, Frauenfeld OW, Nair US, Fall S (2014) Land cover changes and their biogeophysical effects on climate. *Int J Climatol* 34:929–953. <https://doi.org/10.1002/joc.3736>
- Miao S, Chen F, LeMone MA, Tewari M, Li Q, Wang Y (2009) An observational and modeling study of characteristics of urban heat island and boundary layer structures in Beijing. *J Appl Meteorol Climatol* 48:484–501. <https://doi.org/10.1175/2008JAMC1909.1>
- Mlawer EJ, Taubman SJ, Brown PD, Iacono MJ, Clough SA (1997) Radiative transfer for inhomogeneous atmospheres: RRTM, a validated correlated-k model for the longwave. *J Geophys Res Atmos* 102:16663–16682. <https://doi.org/10.1029/97JD00237>
- Monaghan AJ, Steinhoff DF, Bruyere CL, Yates D (2014) NCAR CESM global bias-corrected CMIP5 output to support WRF/MPAS research. Research Data Archive at the National Center for Atmospheric Research, Computational and Information Systems Laboratory, Boulder, CO. <https://doi.org/10.5065/D6DJ5CN4>. Accessed 05 May 2019
- Oke TR (1982) The energetic basis of the urban heat Island. *Q J R Meteorol Soc* 108:1–24. <https://doi.org/10.1002/qj.49710845502>
- Perugini L, Caporaso L, Marconi S, Cescatti A, Quesada B, Noblet-Ducoudré N, House JI, Arneth A (2017) Biophysical effects on temperature and precipitation due to land cover change. *Environ Res Lett* 12:053002. <https://doi.org/10.1088/1748-9326/aa6b3f>
- Sailor DJ, Lu L (2004) A top-down methodology for developing diurnal and seasonal anthropogenic heating profiles for urban areas. *Atmos Environ* 38:2737–2748. <https://doi.org/10.1016/j.atmosenv.2004.01.034>
- Shepherd JM (2005) A review of current investigations of urban-induced rainfall and recommendations for the future. *Earth Interact* 9:1–27. <https://doi.org/10.1175/EI156.1>
- Shi ZT, Xu XY, Jia GS (2021) Urbanization magnified nighttime heat waves in China. *Geophys Res Lett.* <https://doi.org/10.1029/2021GL093603>
- Shimadera H, Kondo A, Shrestha KL, Kitaoka K, Inoue Y (2015) Numerical evaluation of the impact of urbanization on summertime precipitation in Osaka, Japan. *Adv Meteorol.* <https://doi.org/10.1155/2015/379361>
- Skamarock WC, Klemp JB, Dudhia J, Gill DO, Barker DM, Duda MG, Huang XY, Wang W, Powers JG (2008) A Description of the Advanced Research WRF Version 3. NCAR Tech. Note NCAR/TN-475+STR. <https://doi.org/10.5065/D68S4MVH>
- Stocker TF, Qin D, Plattner G-K et al (2014) Climate Change 2013: The physical science basis. Contribution of Working Group I to the Fifth Assessment Report of IPCC the Intergovernmental Panel on Climate Change. Cambridge University Press.
- Sun Y, Zhang XB, Zwiers FW, Song LC, Wan H, Hu T, Yin H, Ren GY (2014) Rapid increase in the risk of extreme summer heat in eastern China. *Nat Climate Change* 4(12):1082–1085. <https://doi.org/10.1038/nclimate2410>
- Sun Y, Zhang XB, Ding YH, Chen DL, Qin DH, Zhai PM (2021) Understanding human influence on climate change in China. *Natl Sci Rev.* <https://doi.org/10.1093/nsr/nwab113>
- Tewari M, Chen F, Wang W, Dudhia J, LeMone M, Mitchell K, Ek M, Gayno G, Wegiel J, Cuenca R (2004) Implementation and verification of the unified NOAH land surface model in the WRF model. In: 20th conference on weather analysis and forecasting/16th conference on numerical weather prediction, pp 11–15. <https://staff.ucar.edu/browse/people/7309/OSGC-000-000-008-560>
- Wang J, Feng JM, Yan ZW, Hu YH, Jia GS (2012) Nested high-resolution modeling of the impact of urbanization on regional climate in three vast urban agglomerations in China. *J Geophys Res Atmos* 117:D21103. <https://doi.org/10.1029/2012JD018226>
- Wang X, Liao J, Zhang J, Shen C, Chen W, Xia B, Wang T (2013) A numeric study of regional climate change induced by urban expansion in the pearl river delta, China. *J Appl Meteorol Climatol* 53:346–362. <https://doi.org/10.1175/JAMC-D-13-054.1>
- Wang X, Sun X, Tang J, Yang X (2015) Urbanization-induced regional warming in Yangtze River delta: potential role of anthropogenic heat release. *Int J Climatol* 35:4417–4430. <https://doi.org/10.1002/joc.4296>
- Wang J, Huang B, Fu DJ, Atkinson PM, Zhang XZ (2016) Response of urban heat island to future urban expansion over the Beijing–Tianjin–Hebei metropolitan area. *Appl Geogr* 70:26–36. <https://doi.org/10.1016/j.apgeog.2016.02.010>
- Wang YJ, Chen LT, Song ZY, Huang ZQ, Ge EJ, Lin LJ, Luo M (2019) Human-perceived temperature changes over south china: long-term trends and urbanization effects. *Atmos Res* 215:116–127. <https://doi.org/10.1016/j.atmosres.2018.09.006>
- Wang J, Feng JM, Yan ZW, Chen Y (2020) Future risks of unprecedented compound heat waves over three vast urban agglomerations in China. *Earth's Future.* <https://doi.org/10.1029/2020EF001716>
- Wang J, Chen Y, Liao WL, He GH, Tett FBS, Yan ZW, Zhai PM, Feng JM, Ma WJ, Huang CR, Hu YM (2021) Anthropogenic emissions and urbanization increase risk of compound hot extremes in cities. *Nat Clim Change.* <https://doi.org/10.1038/s41558-021-01196-2>
- Yang XC, Hou YL, Chen BD (2011) Observed surface warming induced by urbanization in east China. *J Geophys Res* 116:D14113. <https://doi.org/10.1029/2010JD015452>
- Yang B, Zhang YC, Qian Y (2012) Simulation of urban climate with high-resolution WRF model: a case study in Nanjing, China. *Asia Pacific J Atmos Sci* 48(3):227–241. <https://doi.org/10.1007/s13143-012-0023-5>
- Yang GW, Ren GY, Zhang PF, Xue XY, Tysa SK, Jia WQ, Qin Y, Zheng X, Zhang SQ (2021) PM2.5 influence on Urban Heat Island

- (UHI) effect in Beijing and the possible mechanisms. *J Geophys Res Atmos.* <https://doi.org/10.1029/2021JD035227>
- Ye HY, Huang ZQ, Huang LL, Lin LJ, Luo M (2018) Effects of urbanization on increasing heat risks in South China. *Int J Climatol* 38:5551–5562. <https://doi.org/10.1002/joc.5747>
- Zhang N, Gao ZQ, Wang XM, Chen Y (2010) Modeling the impact of urbanization on the local and regional climate in Yangtze River Delta, China. *Theor Appl Climatol* 102:331–342. <https://doi.org/10.1007/s00704-010-0263-1>

Publisher's Note Springer Nature remains neutral with regard to jurisdictional claims in published maps and institutional affiliations.